JOURNAL OF GEOPHYSICAL RESEARCH, VOL. 114, D00D06, doi:10.1029/2008JD011263, 2009

Significant decadal brightening of downwelling shortwave in the continental United States

C. N. Long,[1] E. G. Dutton,[2] J. A. Augustine,[2] W. Wiscombe,[3] M. Wild,[4] S. A. McFarlane,[1] and C. J. Flynn[1]

Received 8 October 2008; revised 14 January 2009; accepted 30 January 2009; published 8 April 2009.

[1] We conduct analyses of all-sky and clear-sky surface downwelling shortwave radiation and bulk cloud properties using data from several Department of Energy Atmospheric Radiation Measurement (ARM) Program and National Oceanic and Atmospheric Administration Surface Radiation (SURFRAD) network sites spanning the years 1995 through 2007. Five ARM sites are aggregated to study downwelling shortwave tendencies on global circulation model grid scales, and then six SURFRAD sites plus the central ARM site are aggregated to study the wider scale of the continental United States. We show that widespread brightening has occurred over the continental United States as represented by these measurements over the 12 years of the study, averaging about 8 W m^{-2}/decade for the all-sky shortwave and 5 W m^{-2}/decade for the clear-sky shortwave. This all-sky increase is substantially greater than the 2 W m^{-2}/decade previously reported over much more of the globe as represented by data from the Global Energy Balance Archive spanning 1986–2000 and is more than twice the magnitude of the corresponding 1986–2000 2–3 W m^{-2}/decade increase in downwelling longwave. Our results show that changes in dry aerosols and/or direct aerosol effects alone cannot explain the observed changes in surface shortwave (SW) radiation, but it is likely that changes in cloudiness play a significant role. These SW increases are accompanied by decreasing tendencies in cloudiness, and an increasing tendency in the clear-sky SW diffuse/direct ratio that is often associated with atmospheric turbidity. However, given the many local influences, evidence presented here suggests that the determination of the causes of decadal changes in the downwelling solar radiation at the surface are better studied locally and regionally, rather than on a global or continental scale.

Citation: Long, C. N., E. G. Dutton, J. A. Augustine, W. Wiscombe, M. Wild, S. A. McFarlane, and C. J. Flynn (2009), Significant decadal brightening of downwelling shortwave in the continental United States, *J. Geophys. Res.*, *114*, D00D06, doi:10.1029/2008JD011263.

1. Introduction

[2] Several recent studies have shown evidence of a widespread decrease in downwelling solar radiation reaching Earth's surface from roughly the 1960s through the late 1980s or early 1990s [*Ohmura and Lang*, 1989; *Gilgen et al.*, 1998; *Stanhill and Cohen*, 2001; *Liepert*, 2002; *Wild et al.*, 2004], at least over land surfaces. This multidecadal decreasing surface solar radiation trend has been called "global dimming" in reference to the global (total) downwelling shortwave radiation measurements the studies were based on. More recent work shows evidence that to the extent that there was a general "dimming" trend it had evolved into a "brightening" during the later 1990s into the 2000s [*Wild et al.*, 2005; *Pinker et al.*, 2005; *Dutton et al.*, 2006]. *Wild et al.* [2005] show an aggregate decadal increase of 6–7 W m^{-2}/decade from eight globally distributed BSRN (Baseline Surface Radiation Network) sites spanning from 1992 to 2002 which is, however, partly due to recovery from the Mount Pinatubo eruption. *Wild et al.* [2008] show a smaller decadal increase over much of the globe as represented by data from the Global Energy Balance Archive [*Gilgen et al.*, 1998] spanning 1986–2000 when the Pinatubo affected years are neglected. Their estimated 1986–2000 brightening is of similar magnitude to the preceding decadal rate of dimming estimated at a decrease of about 2–3 W m^{-2}/decade over the three decades from 1960 to 1990 [*Wild et al.*, 2004], while the more recent Pinatubo-influenced (1990s) rate of increase [*Wild et al.*, 2005] is 3 times the magnitude of the preceding decadal rate of dimming.

[3] Arguments have been made that the decades of dimming may have to some extent offset expected global warming due to greenhouse gases [*Wild et al.*, 2007;

[1]Climate Physics Group, Pacific Northwest National Laboratory, Richland, Washington, USA.
[2]Global Monitoring Division, ESRL, NOAA, Boulder, Colorado, USA.
[3]Brookhaven National Laboratory, Upton, New York, USA.
[4]Institute for Atmospheric and Climate Science, Eidgenossische Technische Hochschule, Zurich, Switzerland.

0148-0227/09/2008JD011263$09.00

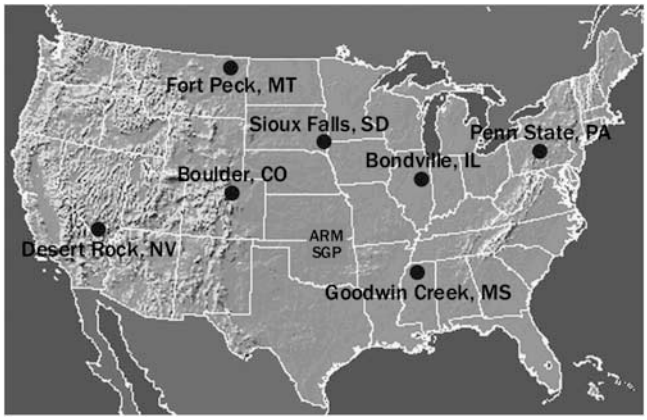

Figure 1. Map of the continental United States showing the area covered by the ARM SGP network in north central Oklahoma and south central Kansas, and the locations of the various SURFRAD sites.

Ruckstuhl et al., 2008], with the more recent brightening now contributing to more rapid manifestations of global greenhouse warming effects and possibly to the recent acceleration of the land-based hydrological cycle [*Wild et al.*, 2008]. The 2007 Intergovernmental Panel on Climate Change Assessment Report (IPCC AR-4) [*IPCC*, 2007] estimate of the global average net anthropogenic greenhouse radiative forcing of on average 1.6 W m^{-2} and an upper bound at 2.4 W m^{-2}, though this estimate is in reference to the tropopause and is difficult to relate to surface effect owing to our lack of understanding of the many interrelated atmospheric forcings and feedbacks involved. However, *Wild et al.* [2008] do report a widespread 2–3 W m^{-2}/decade increase in surface downwelling longwave from 1986 to 2000 which is of comparable magnitude to their reported corresponding shortwave increases for the same period. The more recent 1992–2002 shortwave increase of 6–7 W m^{-2}/decade is more than twice the corresponding 2–3 W m^{-2}/decade magnitude increase of the surface downwelling longwave for the same period. Thus ''global dimming and brightening'' (GDB), defined as decadal changes in the amount of solar radiation reaching the Earth's surface, becomes an important consideration for studies of the climatological component of the Earth's radiation balance. To predict GDB for climate change, we must understand the causes that produce the effect. While some researchers promote changes in aerosol amounts as the primary cause of GDB [e.g., *Norris and Wild*, 2007; *Streets et al.*, 2006], other studies indicate that clouds perhaps play a significant role [e.g., *Ruckstuhl et al.*, 2008]. We present here an assessment of GDB using surface radiation measurement sites sparsely spread across the continental United States, both for all- and clear-sky irradiances, as well as investigations as to the changes in other variables related to surface downwelling solar radiation in an attempt to determine causes for the changes indicated in the data record.

2. Data and Methodology

[4] For this study, data from both the Department of Energy Atmospheric Radiation Measurement (ARM) and National Oceanic and Atmospheric Administration continental U.S. sites are used. Data from the ARM Climate Research Facility (ACRF) are from the Southern Great Plains (SGP) network located roughly in north central Oklahoma and south central Kansas (see Figure 1 and Table 1 for a list of sites and locations). The surface radiation data are from Solar Infrared Radiation Station systems at the network Extended Facilities and a combined ARM Value Added Product called the Best Estimate Flux (the BEF data) for the Central Facility of the SGP ACRF site. The BEF algorithm analyzes the data from three available collocated radiation systems to produce a best estimate of the broadband irradiances, in general by averaging the two out of the three measurements that agree best at any given time [*Shi and Long*, 2002]. These radiation systems use Eppley Normal Incidence Pyrheliometers (NIP), Precision Spectral Pyranometers (PSP), and shaded Model 8–48 ''Black and White'' pyranometers (B&W) for the shortwave (SW) measurements, and Eppley Precision Infrared Radiometers (PIR) for the longwave (LW) to produce 1-min averages. (Details about these radiation systems and the instruments used are available at www.arm.gov.) Estimates of the 2-sigma uncertainties of the measurements are 3% or 4 W m^{-2}, 6% or 20 W m^{-2}, 6% or 10 W m^{-2}, and 2.5% or 4 W m^{-2} (whichever value, the given W m^{-2} or percent of signal, is largest for each) for the downwelling direct normal SW, diffuse SW, total SW, and LW, respectively [*Stoffel*, 2005]. However, it should be noted that it is long-term precision, which is generally considered to be a subset of absolute accuracy, which is most important to our long-term analyses. The total downwelling SW used in this study is primarily the sum of the direct plus diffuse components whenever available; otherwise the global SW from the unshaded Eppley PSP is used. All radiometers are replaced yearly with freshly calibrated units, and domes at the SGP Central Facility are cleaned daily with those at the Extended Facilities serviced biweekly. Instrument performance is monitored on a daily basis to ensure data quality [*Peppler et al.*, 2008] with maintenance as needed to assure the best possible data continuity. The air temperature and humidity measurements (used in the calculation of clear-sky downwelling LW) are from the ARM Surface Meteorological Observation Systems, which use a Campbell Scientific Model HMP35C temperature and humidity probe (manufactured by Vaisala) in an aspirated enclosure. The estimated uncertainty is 0.6°C for air temperature, and 2–3% for relative humidity (RH) [*Ritsche*, 2006].

[5] Data from the NOAA U.S. Surface Radiation Budget Network (SURFRAD) are also used for this study [*Augustine et al.*, 2000, 2005]. The network comprises seven stations that sample different climates throughout the 48 contiguous states in Illinois, Montana, Mississippi, Colorado, Pennsylvania, Nevada, and South Dakota (see Table 1). SURFRAD has been operational since 1995. Downwelling SW is measured by combining direct and diffuse solar measurements made with an Eppley NIP and shaded Eppley B&W, respectively. Global SW is also measured with a Spectrolab model SR-75 pyranometer and is used as a backup if the solar tracker fails. Upwelling, or reflected, SW is measured with an inverted Spectrolab model SR-75 pyranometer on a 10-m tower. Downwelling and upwelling thermal LW are measured with Eppley PIRs. Uncertainties of these basic

Table 1. Listing of Sites Whose Data Were Used in This Study

Network	Site Identification	Name	Latitude (°N)	Longitude (°W)	Kilometers From SGP Central Facility
ARM SGP	C1	Central Facility	36.61	97.49	0
ARM SGP	E07	Elk Falls, Kans.	37.38	96.18	145
ARM SGP	E08	Coldwater, Kans.	37.33	99.31	181
ARM SGP	E20	Meeker, Okla.	35.56	96.99	124
ARM SGP	E24	Cyril, Okla.	34.88	98.21	202
SURFRAD	BON	Bondville, Ill.	40.06	88.37	883
SURFRAD	DRA	Desert Rock, Nev.	36.63	116.02	1654
SURFRAD	FPK	Fort Peck, Mont.	48.31	105.10	1444
SURFRAD	GWN	Goodwin Creek, Miss.	34.25	89.87	738
SURFRAD	PSU	Penn State Univ., Pa.	40.72	77.93	1758
SURFRAD	TBL	Table Mountain, Colo.	40.13	105.24	781

surface radiation budget measurements are given by *Augustine et al.* [2000] for the pyranometers (Spectrolab, PSPs and 8–48s) as 2–5%, for the NIPs as 2–3%, and for the PIRs as 9 W m^{-2}. Five spectral SW channels from a MultiFilter Rotating Shadowband Radiometer (MFRSR) [*Harrison et al.*, 1994] are used to generate an aerosol optical depth (AOD) product [*Augustine et al.*, 2008]. Other measurements include wind speed and direction, air temperature, relative humidity, and station pressure. Accuracy of the Vaisala model HMP50 temperature and relative humidity probe is 0.5°C for temperature, and 2–3% for RH below 90% RH or 6% above 90% RH. All measurements but AOD are 3-min averages of 1-s samples. The resolution of the AOD measurements varies depending on the source of the MFRSR data, although most are 2-min averages. Quality assurance practices are applied to keep SURFRAD data as continuous as possible. For example, instruments at SURFRAD stations, except the MFRSR, are exchanged annually with freshly calibrated units. Data loggers are calibrated every 3 years, and other equipment with limited lifetimes, such as multiplexers and ventilator fans, are replaced on a regular schedule.

[6] For both the ARM and SURFRAD networks, shaded PSPs (or in some cases SR-75s for SURFRAD) were used for diffuse SW measurements in the earlier years of the records. These "single black detector" diffuse SW measurements are known to suffer from infrared (IR) loss from the detectors, thus producing a low bias in the measurements [*Dutton et al.*, 2001; *Philipona*, 2002]. Most of these shaded PSPs were replaced during 1999 with Eppley B&W pyranometers, which have negligible offset. For the periods that the shaded single black detectors were used for the diffuse measurement, a correction for IR loss has been applied. For the ARM data, the correction methodology of *Younkin and Long* [2004] was used. For the SURFRAD data, a modified form of the *Dutton et al.* [2001] method was applied, as described by *Augustine et al.* [2005]. Global SW measurements by single black detector pyranometers also are affected by infrared loss of about the same magnitude as the diffuse measurement. They also include a "cosine" error that tends to decrease the signal. The cosine error results mainly from differential reflection of the beam by the detector surface as a function of solar zenith angle, among other effects, and therefore is only effective when the direct solar beam is present. These errors are both negative and are not corrected for in the SURFRAD global SW measurements analyzed, but are corrected in the ARM data using the same methodology as for the diffuse PSP data. These errors do not affect the measurements combined for the component sum irradiance, i.e., diffuse plus direct SW, which is our primary source of downwelling SW data.

[7] All radiation data used for this study has been quality tested using the QCRad methodology of *Long and Shi* [2008]. QCRad in essence uses climatological analyses of the surface radiation measurements themselves to define reasonable limits for testing the data for unusual data values. The methodology not only sets fairly standard maximum and minimum value limits, but includes many cross comparisons based on experience gained regarding instrument behavior in the field in development of ARM Value Added Products (VAPs) such as the Diffuse IR Loss Correction VAP [*Younkin and Long*, 2004] and the Best Estimate Flux VAP [*Shi and Long*, 2002].

[8] After quality testing, the Radiative Flux Analysis processing, a collection of analysis tools used to produce continuous clear-sky (i.e., cloudless sky) estimates and infer bulk cloud properties from surface radiation data, is applied. The Radiative Flux Analysis produces value added information such as detected clear-sky periods and continuous clear-sky estimates of SW [*Long and Ackerman*, 2000; *Long and Gaustad*, 2004], and LW [*Long*, 2004; *Long and Turner*, 2008] irradiances, total daylight fractional sky cover [*Long et al.*, 2006], cloud effective transmissivity and visible optical depths [*Barnard and Long*, 2004; *Barnard et al.*, 2008], cloud downwelling radiating temperature, and the complete net surface radiative cloud forcing [*Long*, 2005].

[9] Seasonal and yearly averages were produced with the measured and estimated parameters of the Radiative Flux Analysis. These averages were produced by first collecting all data into the appropriate 15-min bins across the 24-h daily period, then producing an average diurnal cycle. The resultant diurnal cycle is then averaged to produce the seasonal and annual average values. For instance, all data for the year 2004 is binned for the 24 h at 15-min resolution, and then a yearly average diurnal cycle is calculated. The resultant yearly average diurnal cycle is then averaged across the 24 h to produce the 2004 yearly average. In this way the effects of missing or bad data are minimized while at the same time avoiding the practice of manufacturing values to "fill in" for missing values.

[10] We use the seasonal and yearly averages to look for the most apparent changes across the time period under study, spanning from 1995 through 2007 for all available

Table 2. Listing of Results for Time Series That Passed the Mann-Kendall Linear Significance Testing[a]

Variable	MK-Sen Slope	95% Min	95% Max	*p*	Figure
SGP CF Yearly Averages					
All-sky total SW	0.7595	0.0247	1.5893	0.0190	2
All-sky diffuse SW	0.4467	0.0427	0.8351	0.0142	3
Clear-sky diffuse SW	0.3208	0.0890	0.6376	0.0053	3
Clear-sky SW diffuse/direct ratio	0.0016	0.0003	0.0029	0.0062	6
SGP CF Seasonal Averages					
Spring clear-sky diffuse SW	0.3000	−0.0114	0.6469	0.0205	N/A
Spring clear-sky SW diffuse/direct ratio	0.0012	0.0000	0.0031	0.0205	10
Summer clear-sky total SW	0.5425	0.0987	1.3016	0.0140	9
Fall clear-sky total SW	0.7250	0.1104	1.2823	0.0140	9
Fall all-sky diffuse SW	0.4750	0.1607	0.7625	0.0030	N/A
SGP Area Sites Yearly Averages					
Clear-sky total SW	0.4269	0.1349	0.6229	0.0008	11
U.S. All-Sites Yearly Averages					
All-sky total SW	0.7384	0.2890	1.2440	0.0014	13
Clear-sky total SW	0.5389	0.1256	0.8666	0.0062	17
All-sky diffuse SW	0.4983	0.0205	0.8280	0.0062	14
Clear-sky diffuse SW	0.4485	0.2563	0.6399	0.0000	18
All-sky direct SW	0.5869	0.0149	1.1678	0.0142	14
Clear-sky SW diffuse/direct ratio	0.0023	0.0010	0.0031	0.0000	19

[a]MK-Sen slope refers to the slope estimate using the methodology of *Sen* [1968], 95% Min and 95% Max represent the slope minimum and maximum 95% confidence level, *p* refers to the two-sided level of significance (p value), Figure is the figure number of the corresponding data plot, and N/A denotes not applicable.

data. Least squares linear fitting is used to investigate the overall tendencies during the time period. We also determine whether the slope estimates represent a statistically significant trend by using the Mann-Kendall (MK) method of significance determination [*Mann*, 1945; *Kendall*, 1975] along with the related slope determination following *Sen* [1968], as developed and utilized by *Hirsch et al.* [1982] and others. This methodology has gained rather wide acceptance in hydrometeorological applications as discussed by *Yue et al.* [2002].

[11] Our computations were carried out using the commercially available SYSTAT12 ™ (2007) statistical analysis package. The nonparametric MK method combined with Sen's trend estimates provides a more rigorous determination of significance because fewer limitations are placed on the nature of the data as compared to ordinary least squares fitting uncertainty estimates. The MK method is based on a mean determination of the number of point to point changes in the data compared to that expected when there is no trend in the data. The significance of this trend test is based on a normally distributed test statistic such that if the number of observations is greater than about 9 the normal distribution probability curves and tables can be used. The computed trends here are determined to be significant if a two-sided level of significance (p value) of 0.025 or less is achieved, and the estimated 95% slope uncertainty limits do not include 0.0. The Sen's slope 95% confidence intervals found here are rather wide, which is indicative of the relatively short data series and substantial year-to-year variability in the data. The MK results and Sen's slopes for all time series used in this study that passed the above significance tests are listed in Table 2. Note that the Sen's estimated slope values differ to some extent from those of the least squares fitting given in Figures 2, 3, 9–11, 13, 14, and 17–19 owing to the differing slope estimation methodologies used, but that there is substantially little difference between the two, with both slope estimates being much closer to each other than the 95% limits.

3. Results for the ARM SGP Central Facility

[12] We use the ARM Best Estimate Flux value-added product for the SGP Central Facility data, which has three-radiometer redundancy. Figure 2 shows the yearly averages of the all- and clear-sky downwelling SW, along with the corresponding least squares linear fit. In both cases there is a tendency for the SW to increase in the aggregate across the study years, with the all-sky SW trend (6 W m^{-2}/decade) passing the MK tests for significance (Table 2) and being about twice that of the clear-sky increase (3 W m^{-2}/decade). Looking at the components of the downwelling SW (Figure 3), both the all-sky direct and diffuse components exhibit an increasing tendency with the diffuse SW (5 W m^{-2}/decade) passing the MK test for linear trend significance and increasing more than the direct SW (1 W m^{-2}/decade). For clear skies the direct SW effectively shows no change, while the diffuse SW increases (3 W m^{-2}/decade) and again passes the MK test for linear trend significance.

[13] Figure 4 shows the yearly average daylight fractional sky cover derived from the SW measurements [*Long et al.*, 2006], and the daily average LW "effective" sky cover derived from the LW measurements using a method adapted from *Durr and Philipona* [2004]. The LW-derived sky cover is termed "effective" given that it represents primarily the low and middle cloudiness since the broadband downwelling LW is not significantly influenced by high, cold clouds [*Long and Turner*, 2008], where the SW derived sky cover represents total cloudiness, but is available only during daylight. In both cases there is a tendency for decreasing cloudiness, of −2%/decade in SW total sky

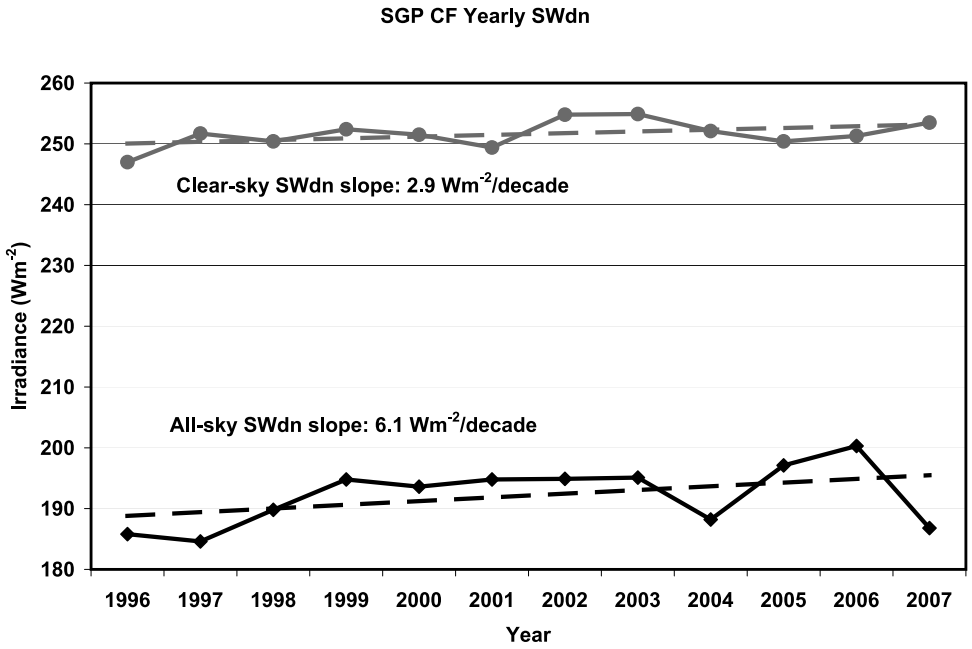

Figure 2. Yearly averages of all-sky (black) and clear-sky (gray) downwelling SW for the ARM SGP Central Facility, along with their corresponding least squares linear fits.

cover. This is anticorrelated with the increasing trend for all-sky SW (Figure 2), suggesting that changes in cloud amount are likely playing a role in the changes in all-sky downwelling SW, especially given the larger magnitude changes in all-sky SW compared to the clear-sky SW. This assertion is supported in Figure 5 showing that the effect of clouds on the downwelling SW, calculated as the clear-sky minus the measured SW, tends to decrease in magnitude over the years. The decreasing tendency of the LW effective low and middle cloudiness (Figure 4) is greater across the study years than that for SW total cloudiness, which suggests changing tendencies in not only the overall cloud amount but the gross vertical distribution of cloudiness as well. Note that the SW sky cover retrievals use diffuse SW measurements which are part of the total SW and are thus not completely independent of the total SW, though the SW sky cover retrievals have been extensively tested against both sky imager retrievals and human observations which

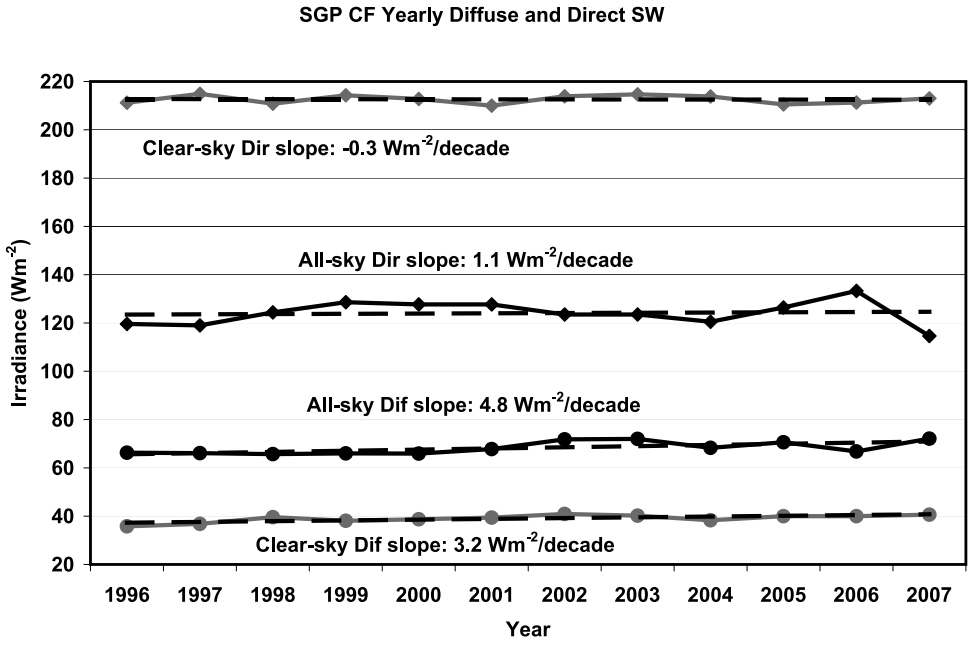

Figure 3. Yearly averages of all-sky direct (black curve with diamonds) and diffuse (black curve with dots) and clear-sky direct (gray curve with diamonds) and diffuse (gray curve with dots) downwelling SW for the ARM SGP Central Facility, along with their corresponding least squares linear fits.

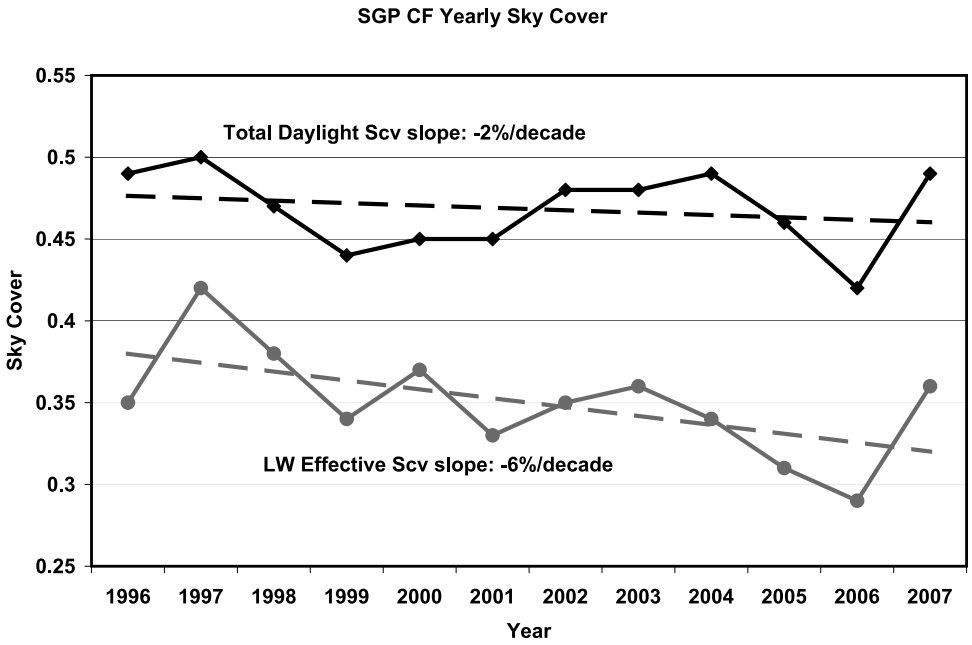

Figure 4. Yearly averages of SW daylight total (black) and daily LW effective (gray) fractional sky cover (Scv) for the ARM SGP Central Facility, along with their corresponding least squares linear fits.

are independent of any SW measurements [*Long et al.*, 2006]. The LW effective sky cover is also independent of any SW measurements, since the retrieval uses only downwelling LW, and screen height (2m) air temperature and humidity measurements [*Long and Turner*, 2008; *Durr and Philipona*, 2004].

[14] For the clear-sky increase in downwelling SW (Figure 2), clouds do not play a role. However, this does not mean that condensed water in the atmosphere, either liquid or solid, has no part. In any separation of "cloudy" versus "clear" there must be some inherent definition of how much condensed water is allowed before a classification of "cloud" is applied. As shown by *Dupont et al.* [2008], a visible optical depth of about 0.15 or less is included in the "clear" classification of the *Long and Ackerman* [2000] methodology, which is consistent with sky imager retrievals and human observations [*Long et al.*, 2006]. These occurrences are primarily high, optically thin subvisual cirrus. It must also be noted that the direct SW component NIP measurements include a roughly 5.5° field-

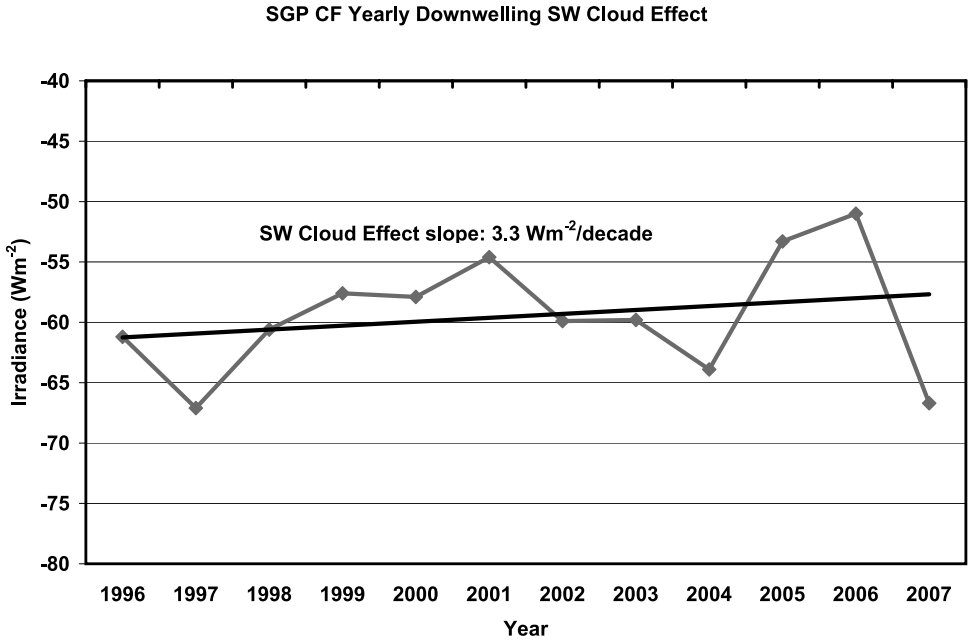

Figure 5. Yearly averages of the downwelling SW cloud effect (all sky minus clear sky) for the ARM SGP Central Facility, along with the corresponding least squares linear fit.

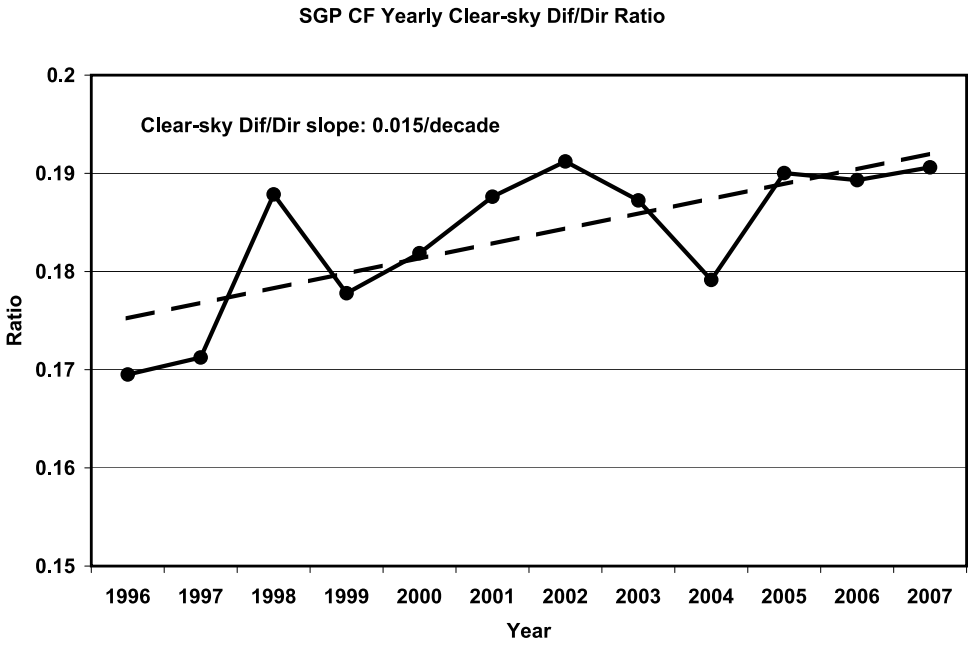

Figure 6. Yearly averages of the ratio of clear-sky diffuse over direct SW for the ARM SGP Central Facility, along with the corresponding least squares linear fit.

of-view, which is not the same as the "direct beam" of a radiative transfer model, and thus includes some irradiance that would be modeled as part of the diffuse SW field. Even retrievals of aerosol optical depths have finite fields-of-view that are usually larger than the solar disk, and include screening for direct solar measurements uncontaminated by "cloud," thus also inherently include some amount of allowed condensed water in the "clear-sky" column. Figure 3 shows the clear-sky direct SW virtually unchanging with the clear-sky diffuse SW increasing. A ratio of the clear-sky diffuse over direct SW is often associated with atmospheric turbidity, but using broadband measurements rather than spectral measurements for which wavelength-dependent aerosol optical depths are retrieved. Figure 6 shows the clear-sky diffuse/direct ratio exhibits an increasing tendency across the study years (0.015/decade), which passes the MK test for linear trend significance. But it cannot be assumed that this trend is caused only by the direct effect of changes in dry aerosols, as there also may be other components such as aerosol indirect effects and/or changes in the atmospheric humidity profile component (such as increased high-altitude air traffic) that produce haze but that is still included in the clear-sky classifications. Obviously further study is needed.

[15] To investigate the magnitude of changes in aerosol properties that would be required to produce the observed increase in diffuse SW at SGP (3 W m^{-2}) we perform a simple model sensitivity test. As a base calculation, we take an aerosol optical depth (0.15 at 500 nm) and Angstrom parameter (1.3) typically found at the SGP site and assume a single scattering albedo (SSA; 0.9 at 500 nm) and asymmetry parameter (AP; 0.5 at 500 nm) that represent the more absorbing range of aerosol properties seen at the SGP [*Michalsky et al.*, 2001, 2006]. The AOD, SSA, and AP vary with wavelength on the basis of the given values at 500 nm and the Angstrom parameter. We calculate the broadband shortwave diffuse and direct downwelling SW every 15 min for the solar geometry of June 21 at SGP using the SHDOM radiative transfer model [*Evans*, 1998] in 1D mode, and average the SW over a 24-h period. The calculated daily average diffuse SW for the base case is 33.3 W m^{-2}. In Table 3 we show the result of several sensitivity studies in which the AOD, SSA and AP are varied. If AOD is held constant, the difference from the base case using the least absorbing values of SSA and AP observed in May at the SGP [*Michalsky et al.*, 2006] produces a 24-h averaged diffuse SW difference of 1.2 W m^{-2}. Increasing AOD to 0.2 and using the less absorbing aerosol optical properties yields a difference of 3.4 W m^{-2} in diffuse SW from the base case. We also do a calculation in which the aerosol optical properties are replaced by optical properties appropriate for cirrus (AOD = 0.15, Angstrom = 0.0, SSA = 0.9999, AP = 0.80), to illustrate the effect of a possible increase in subvisible cirrus that would still be classified as "clear-sky" by the *Long and Ackerman* [2000] methodology [*Dupont et al.*, 2008]. For the same AOD at 500 nm as the base case, the cirrus scattering produces 8.1 W m^{-2} larger diffuse SW due to greater SSA and AP from the larger particles.

[16] One question that arises from these analyses is whether the changes are equally spread across the year, or if there might be a seasonal dependence. To investigate, we divide the year into winter (December–February), spring (March–May), summer (June–August), and fall (September–November) seasons. Figure 7 shows the seasonal all-sky SW results, where indeed differing tendencies occur in the different seasons. The greatest all-sky increase occurs in the fall season (11 W m^{-2}/decade), followed by winter (7–8 W m^{-2}/decade). A decrease is indicated for the spring. These results are again anticorrelated with the corresponding tendencies in SW total sky cover (Figure 8) where the greatest sky cover decrease occurs in winter (−9%/decade), and an increase in cloudiness occurs in

Table 3. Calculated Surface Broadband Diffuse and Direct Shortwave Based on Given Optical Properties[a]

Case Type	AOD	Angstrom	AP	SSA	F_dif (W m^{-2})	F_dir (W m^{-2})	ΔF_dif (W m^{-2})
Aerosol	0.15	1.3	0.50	0.90	33.27	347.77	
Aerosol	0.15	1.3	0.65	0.96	34.44	347.77	1.17
Aerosol	0.1	1.3	0.50	0.90	31.37	350.74	−1.90
Aerosol	0.1	1.3	0.65	0.96	32.15	350.74	−1.12
Aerosol	0.2	1.3	0.50	0.90	35.13	344.83	1.86
Aerosol	0.2	1.3	0.65	0.96	36.69	344.83	3.42
Cirrus cloud	0.15	0.0	0.80	0.9999	41.37	346.40	8.10

[a]F_dif and F_dir are calculated 24-h average diffuse and direct SW, respectively. Results from the aerosol base case are given in the first row. ΔF_dif is the change in diffuse SW from the base case when optical properties are varied.

spring (4%/decade). This again strongly suggests a cloudiness influence in the brightening portion of the GDB phenomenon for the SGP site. For clear-sky (Figure 9) the largest increases occur during summer (6 W m^{-2}/decade) and fall (5 W m^{-2}/decade), which both pass the MK test for linear trend significance, with virtually no change during the winter and spring. The corresponding clear-sky SW component results (not shown) include increasing diffuse SW in all seasons, about double for spring and summer than that for fall and winter and with only the spring diffuse SW marginally passing the MK test for linear trend significance. For the clear-sky direct SW there is an increasing tendency in summer and fall and decreasing direct SW in winter and spring, however none of the direct SW fits pass the MK testing. As Figure 10 shows, these changes in the clear-sky SW components produce increasing diffuse/direct ratio tendencies in all seasons except for fall, which exhibits virtually no tendency, with only the spring marginally passing the MK test for linear trend significance.

4. Results for the ARM SGP Network

[17] We perform the same analyses for four of the ARM Extended Facilities that surround the Central Facility in order to test spatial variability across a domain about the size encompassed by typical global circulation model grid spacing of 100 to 200 km (see Table 1). We use data starting with 1996 since most 1995 data for these Extended Facilities are incomplete. Figure 11 shows the results for the downwelling all- and clear-sky SW for the central and four extended facility stations individually, as well as their aggregate average. For the all-sky case, site E07 (with gray dots) consistently exhibits the lowest magnitude SW, and shows anomalously low values for 1998 and 1999 unlike the other sites. Yet there is a degree of year-to-year pattern similarity for these sites, suggesting that for cloudiness, larger-scale (such as synoptic) factors exhibit a degree of influence. This assertion is supported in Figure 12 showing the yearly average SW daylight total and daily LW effective sky cover, both of which also exhibit a similar degree of year-to-year correlation. In the aggregate, the all-sky SW exhibits an increasing tendency for the domain, shown in Figure 11 as the black dotted line and corresponding dashed line representing the linear fit with a slope of 4 W m^{-2}/decade, though this series does not pass the MK test for linear trend significance. The corresponding decreasing aggregate slopes for the cloudiness are −1%/decade and

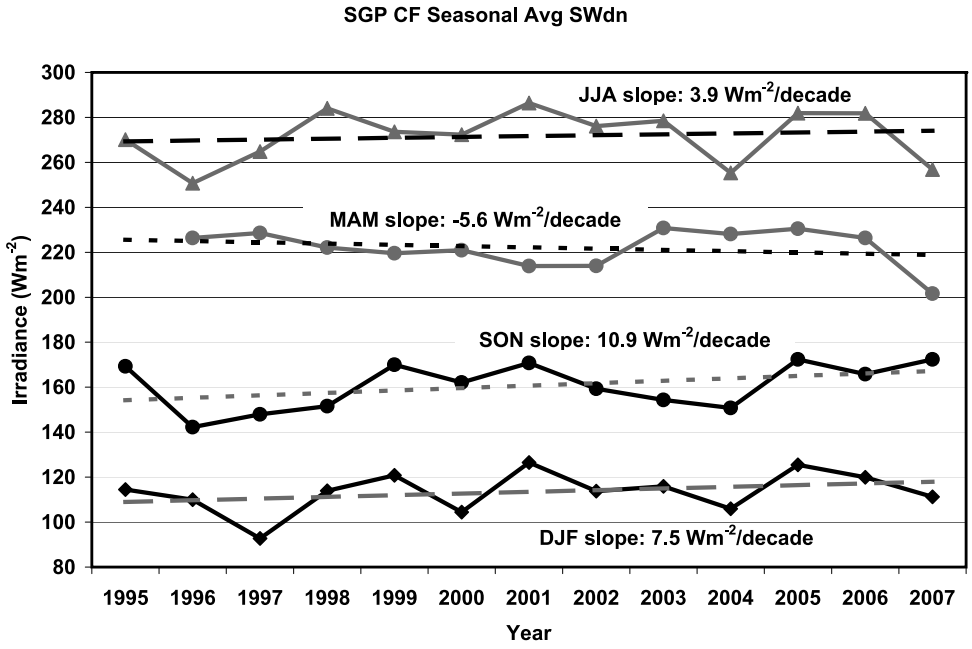

Figure 7. Seasonal averages of downwelling all-sky SW for the ARM SGP Central Facility for winter (black curve with diamonds), spring (gray curve with dots), summer (gray curve with triangles), and fall (black curve with dots), along with the corresponding least squares linear fits.

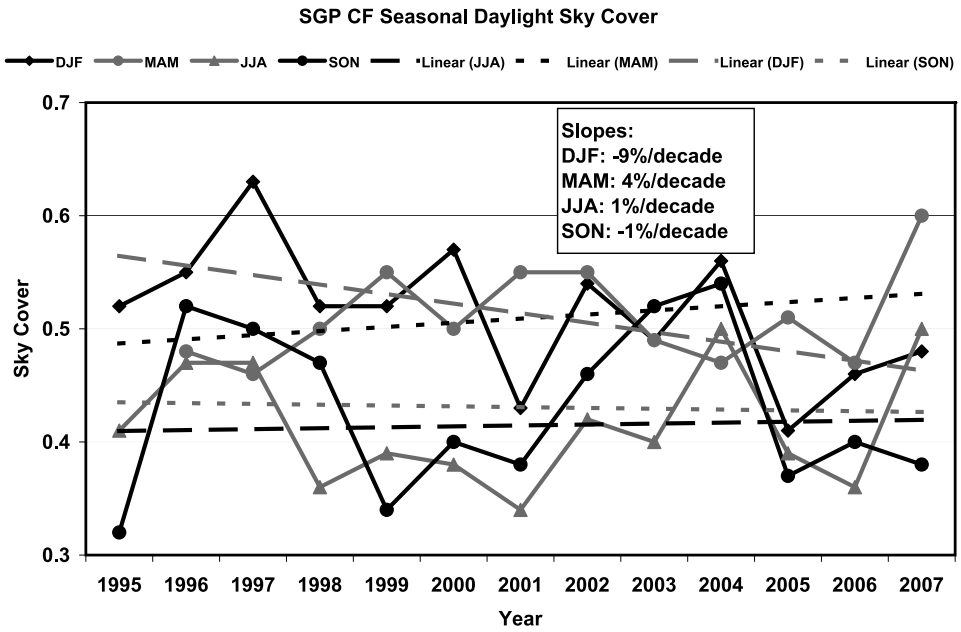

Figure 8. Seasonal averages of SW total daylight sky cover for the ARM SGP Central Facility for winter (black curve with diamonds), spring (gray curve with dots), summer (gray curve with triangles), and fall (black curve with dots), along with the corresponding least squares linear fits.

−2%/decade for the SW total and LW effective sky cover, respectively, again neither passing the MK test for linear trend significance. Only site E24 (Figure 10, with black diamonds) exhibits a decreasing tendency for all-sky SW, with a corresponding increasing tendency of SW total and LW effective sky cover.

[18] For the clear-sky SW in Figure 11, any dependence due to latitude and the resultant yearly average solar elevation angle seems overshadowed by other factors affecting the amount of radiation reaching the surface. Site E24 (with black diamonds) shows the largest clear-sky SW values from 1996 through 1999, which then results in virtually no clear-sky SW tendency across the study years. Since clear sky is included in the all-sky results, this clear-sky result likely plays a role in the E24 all-sky SW decreasing tendency noted above. All other sites exhibit

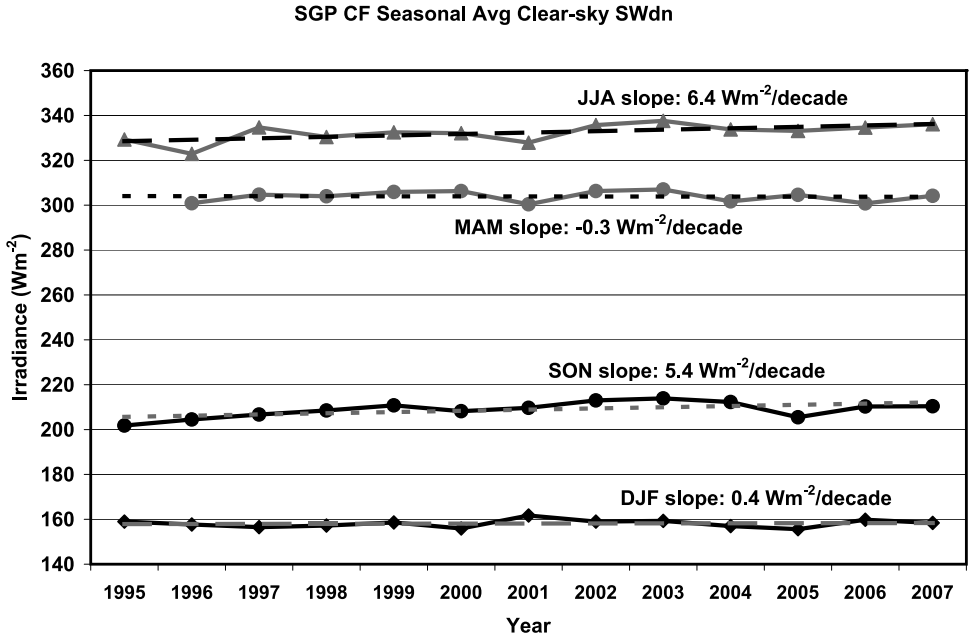

Figure 9. Seasonal averages of downwelling clear-sky SW for the ARM SGP Central Facility for winter (black curve with diamonds), spring (gray curve with dots), summer (gray curve with triangles), and fall (black curve with dots), along with the corresponding least squares linear fits.

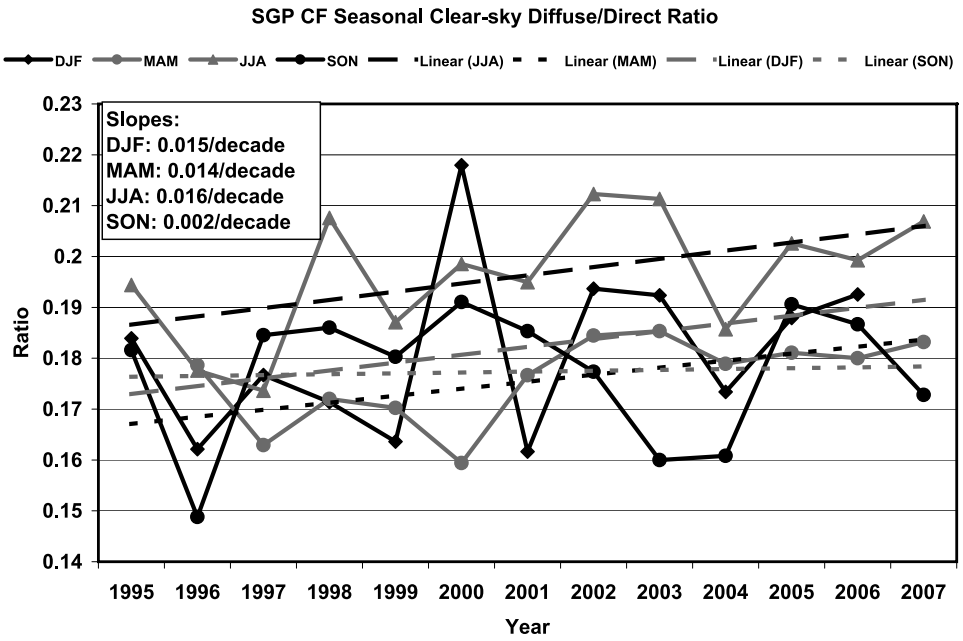

Figure 10. Seasonal averages of SW diffuse/direct ratio for the ARM SGP Central Facility for winter (black curve with diamonds), spring (gray curve with dots), summer (gray curve with triangles), and fall (black curve with dots), along with the corresponding least squares linear fits.

an increasing tendency, with site E08 (with gray dots) having the largest. The aggregate all-site clear-sky SW average passes the MK test for linear trend significance and the resulting slope of 4 W m^{-2}/decade is equivalent to that of the aggregate all-sky SW. But in the clear-sky case there is little temporal correlation between the sites, suggesting that local influences are significantly contributing to the year-to-year variability. For the clear-sky diffuse/direct ratios, besides the Central Facility noted earlier, sites E08 and E24 also exhibit increasing tendencies while sites E07 and E20 show virtually no tendency (not shown). In the aggregate, the diffuse/direct ratio linear fit gives a slope of

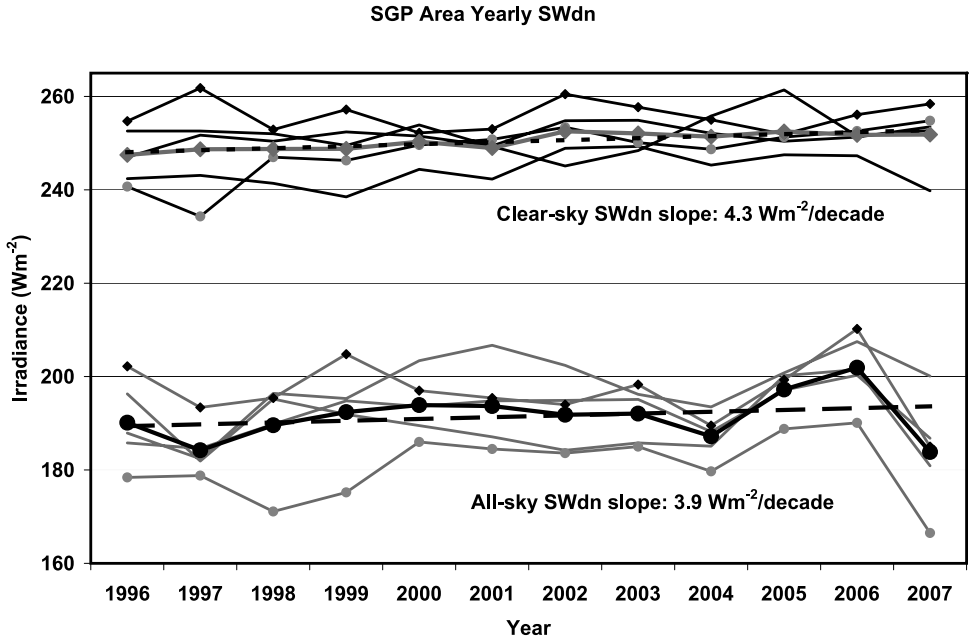

Figure 11. Yearly averages of downwelling all-sky (gray) and clear-sky (black) SW for the ARM SGP Central and Extended Facilities used in this study (see Table 1) as well as the all-sky (black curve with dots) and clear-sky (gray curve with diamonds) aggregate averages and the corresponding least squares linear fits. Site E24 all sky and clear sky denoted with black diamonds added, and E08 clear sky and E07 all sky denoted with gray dots added.

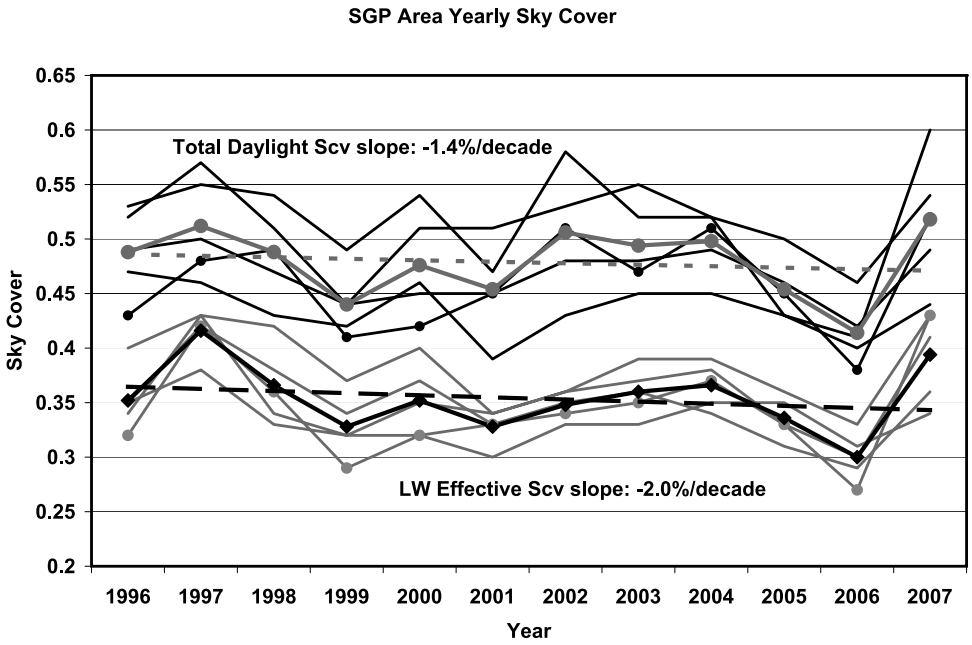

Figure 12. Yearly averages of LW effective (gray) and SW total (black) sky cover (Scv) for the ARM SGP Central and Extended Facilities used in this study (see Table 1) as well as the LW effective (black curve with diamonds) and SW total (gray curve with dots) sky cover aggregate averages and the corresponding least squares linear fits. Site E24 denoted in both with dots added to the line.

0.011/decade out of an overall ratio average value of 0.179, but does not pass the MK test.

5. Results Including the SURFRAD Network

[19] We attempt to investigate the large-scale area of the continental United States by adding six of the SURFRAD sites to the SGP Central Facility (chosen to represent the ARM site). The distances of the SURFRAD sites from the ARM site range from about 740 km for Goodwin Creek to 1760 km for the Penn State site (Table 1). For the SURFRAD sites we again use data starting in 1996, which for most sites was the first full year of operation. The two exceptions are the Desert Rock (DRA) and the Penn State

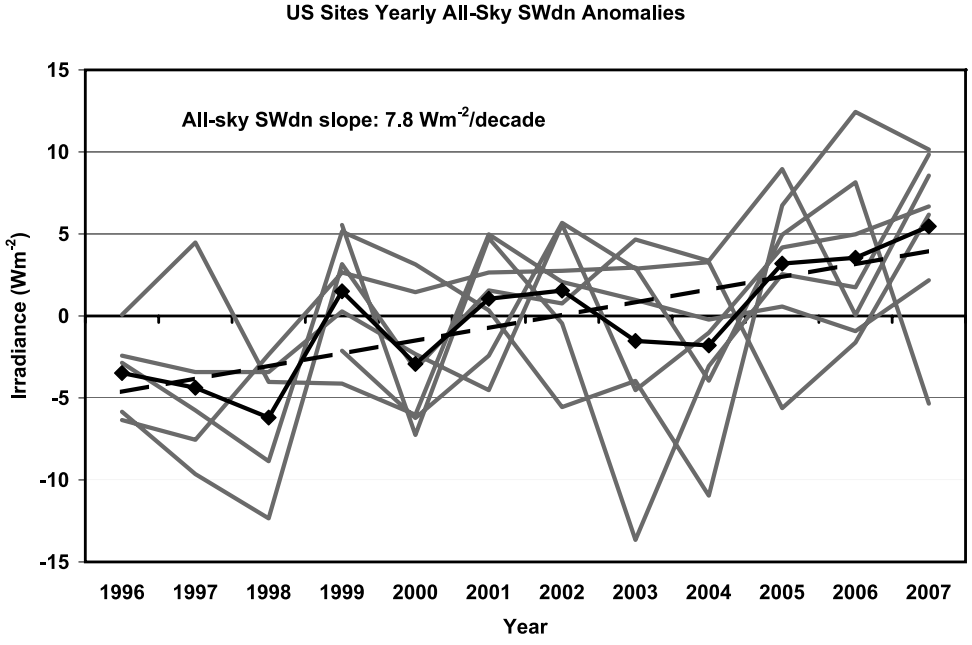

Figure 13. Yearly averages of downwelling all-sky SW anomalies (gray) for the ARM SGP Central Facility and SURFRAD sites used in this study (see Table 1) as well as the all-sky (black curve with diamonds) aggregate average and the corresponding least squares linear fit.

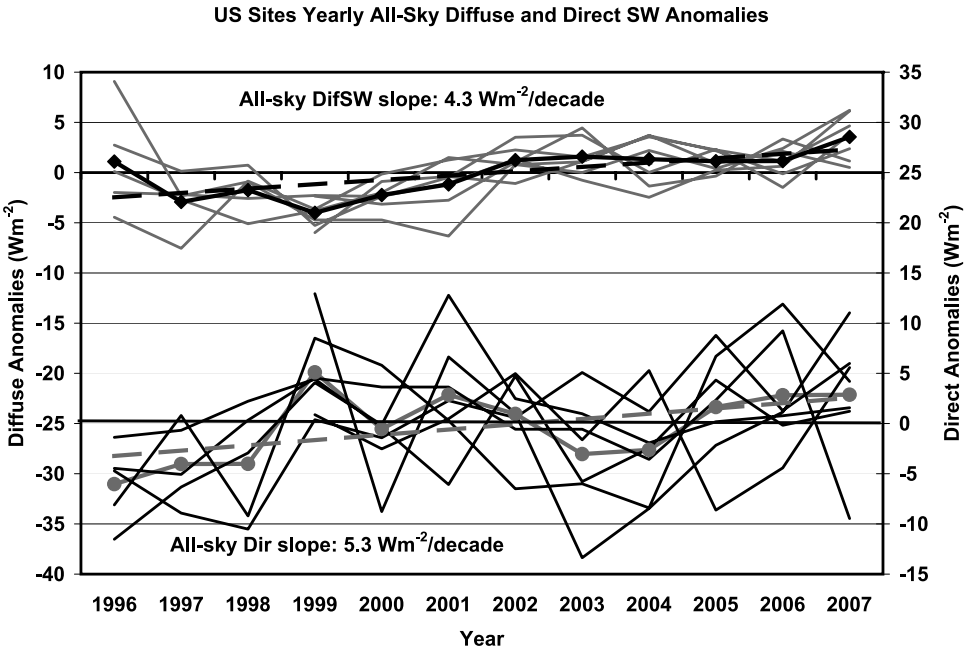

Figure 14. Yearly averages of downwelling all-sky diffuse (gray, left *y* axis) and direct (black, right *y* axis) SW anomalies for the ARM SGP Central Facility and SURFRAD sites used in this study (see Table 1) as well as the all-sky diffuse (black curve with diamonds) and direct (gray curve with dots) aggregate averages and the corresponding least squares linear fits.

University (PSU) sites for which 1999 was the first full year of complete data. Because of the wide range of latitudes, from 34.3°N for Goodwin Creek up to 48.3°N for Fort Peck, we present the data as anomalies from the overall site mean in order to eliminate the effect of solar zenith angle.

[20] Figure 13 shows the composite results for the downwelling all-sky SW anomalies. Anomalies are calculated as the difference from the mean of all years, used to mitigate the large differences between sites in yearly SW magnitudes due to site latitude for the comparison. Bondville exhibits an anomalously low value for 1998, while other anomalously low values occur for Penn State University in 2003, Goodwin in 2004, and the ARM SGP site in 2007. There are anomalously high years for Fort Peck in 1997, Bondville in 2005, and Goodwin in 2006. All sites exhibit an increasing tendency across the study years, with Bondville exhibiting the largest increase at 14 W m^{-2}/decade, and Fort Peck the smallest at 2 W m^{-2}/decade. There is no discernable patterning in these results by either latitude or longitude (not shown). In the aggregate, the all-site average tendency is an increase of 8 W m^{-2}/decade for the least squares linear fit and passes the MK test for linear trend significance.

[21] Figure 14 shows the separate all-sky SW component yearly average anomalies. All sites exhibit an increasing tendency in the diffuse SW: Bondville with the largest at 9 W m^{-2}/decade, and Goodwin and the ARM SGP site the smallest at 3 W m^{-2}/decade. For the direct, the Desert Rock and Penn State University sites are slightly negative (−0.8 W m^{-2}/decade), and the Table Mountain site slightly positive (0.3 W m^{-2}/decade), the three essentially unchanging. All other sites exhibit a positive tendency with the largest for Bondville at 13 W m^{-2}/decade. In the aggregate both the all-site average diffuse and direct SW increase at 4–5 W m^{-2}/decade and both pass the MK test for linear trend significance.

[22] The SW total daylight fractional sky cover yearly average anomalies are shown in Figure 15. The Penn State University site consistently exhibits the greatest average cloudiness, while Desert Rock exhibits by far the least. The Penn State site record produces an increasing tendency across the years at about 2–3% fractional sky cover per decade. All other sites produce a decreasing tendency with the largest at Bondville at −4%/decade, but Table Mountain virtually unchanging with only −0.6%/decade. Overall, the all-site average gives a decreasing tendency of −2%/decade, but does not pass the MK significance testing. Similar results are found with the LW effective sky cover (Figure 16) with again the Desert Rock site consistently having the lowest amount and Penn State the highest, and the all-site average tendency decreasing at about the same rate as the SW total sky cover (−2%/decade) but again does not pass the MK significance testing. Individually, the SGP site exhibits the greatest decreasing tendency at −5%/decade, Penn State again shows an increasing tendency of 5%/decade, and now both Table Mountain and Desert Rock show virtually no tendency across the years for the low and middle cloudiness represented by the LW effective cloud amount.

[23] For the clear-sky case, Figure 17 shows the yearly averages of downwelling SW, while Figure 18 shows the averages for the SW components. Looking at the anomalies of downwelling SW there appears to be a general shift from mostly negative anomalies from 1996 through 2000, little if any anomaly for 2001, and mostly positive anomalies in the following years for all sites. This same pattern is reflected for the clear-sky diffuse SW in Figure 18. This pattern produces about the same aggregate all-site increasing ten-

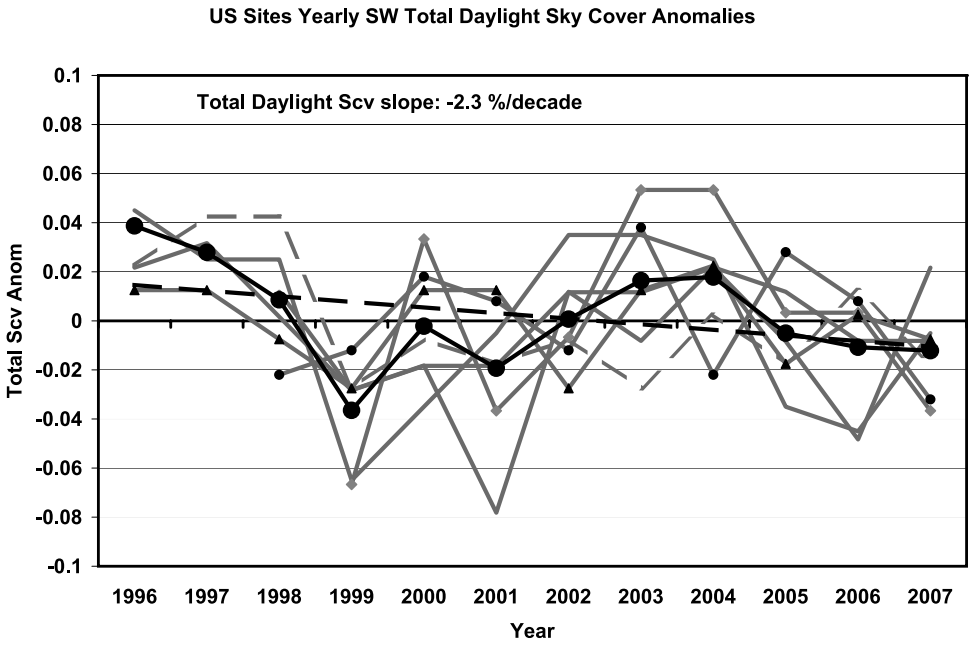

Figure 15. Yearly averages of SW total daylight sky cover (Scv) anomalies (gray) for the ARM SGP Central Facility and SURFRAD sites used in this study (see Table 1) as well as the aggregate average (black curve with dots) and the corresponding least squares linear fit. Individual sites discussed in text denoted as gray diamonds (Penn State), black dots (Desert Rock), black triangles (Table Mountain), and gray dashed curve (Bondville).

dency for the total and diffuse SW at about 5 W m^{-2}/ decade, with both passing the MK significance testing. On the other hand the clear-sky direct SW results are less patterned through time and in the all-site aggregate exhibits virtually no tendency across the study years. Thus, in general, the increase in clear-sky downwelling total SW is produced by an increase in the diffuse SW component. Figure 19 shows the manifestation of these SW component

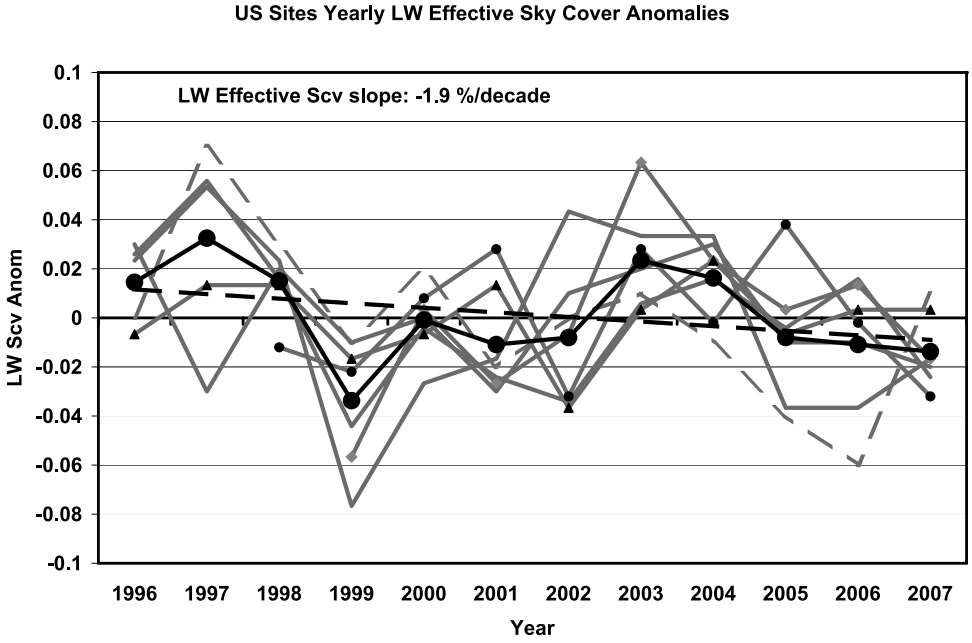

Figure 16. Yearly averages of LW effective sky cover (Scv) anomalies (gray) for the ARM SGP Central Facility and SURFRAD sites used in this study (see Table 1) as well as the aggregate average (black with dots) and the corresponding least squares linear fit. Individual sites discussed in text denoted as gray diamonds (Penn State), black dots (Desert Rock), black triangles (Table Mountain), and gray dashed curve (ARM SP central facility).

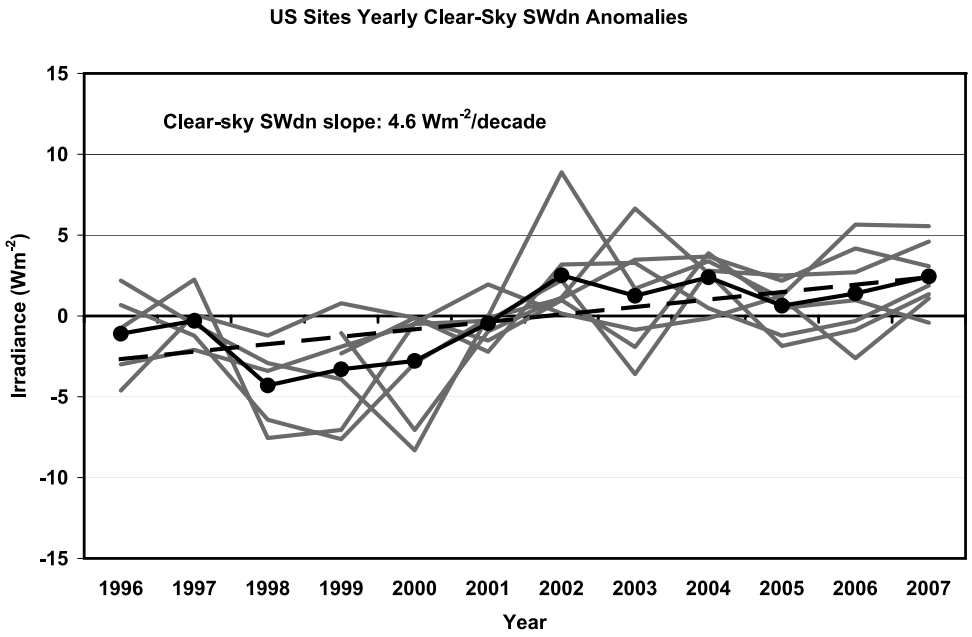

Figure 17. Similar to Figure 13 but for clear-sky downwelling SW.

changes in the SW diffuse/direct ratio which exhibits an increasing tendency for all sites with an aggregate all-site average increase of 0.02/decade which passes the MK significance testing. This result is at odds with the recently published analysis of aerosol optical depth retrievals for the SURFRAD sites [*Augustine et al.*, 2008] that reports that 500-nm aerosol optical depth has decreased over the U.S. SURFRAD sites by about 0.02 units over the 10-year period from 1997 through 2006.

[24] One possible explanation for the disparity between the SURFRAD aerosol optical depth results and the SW diffuse/direct ratio results of this study could be an increase in subvisual cirrus or other haze phenomena. As pointed out previously, the NIP used for direct SW measurements has a relatively wide field-of-view compared to the size of the solar disk. An increase in the occurrences of subvisual cirrus not counted as ''cloud'' (with the attendant large ice crystal size compared with the typical size of dry aerosols) would tend to increase forward scattering and produce a brighter circumsolar disk. *McFarlane and Evans* [2004] used a Monte Carlo radiative transfer model to calculate the amount of the diffuse component that is scattered into the NIP field-of-view by a theoretical cirrus cloud. On the basis of those calculations, for a cirrus cloud composed of

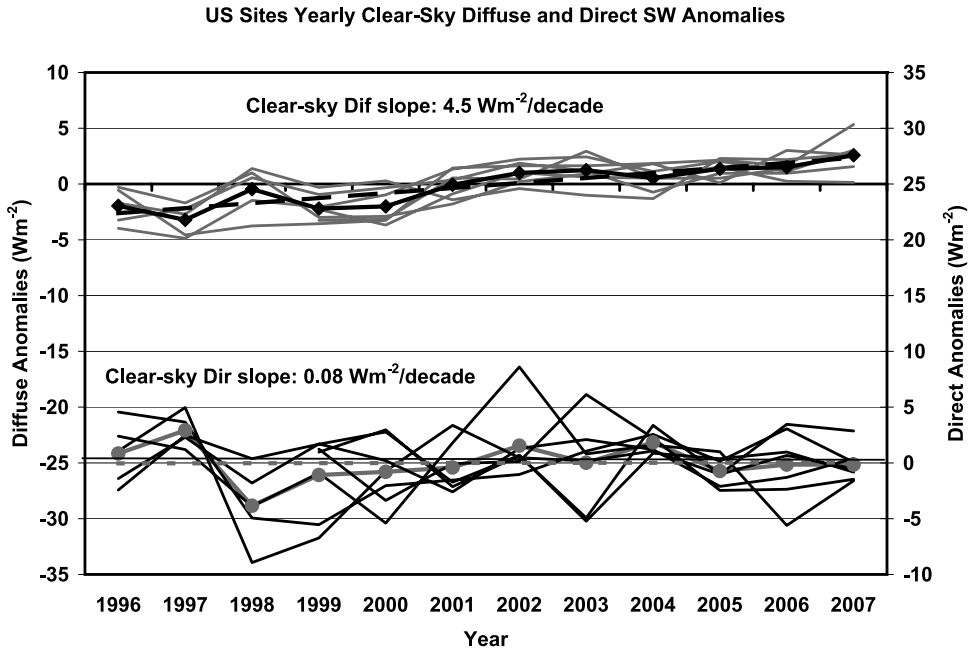

Figure 18. Similar to Figure 14 but for clear-sky diffuse and direct SW.

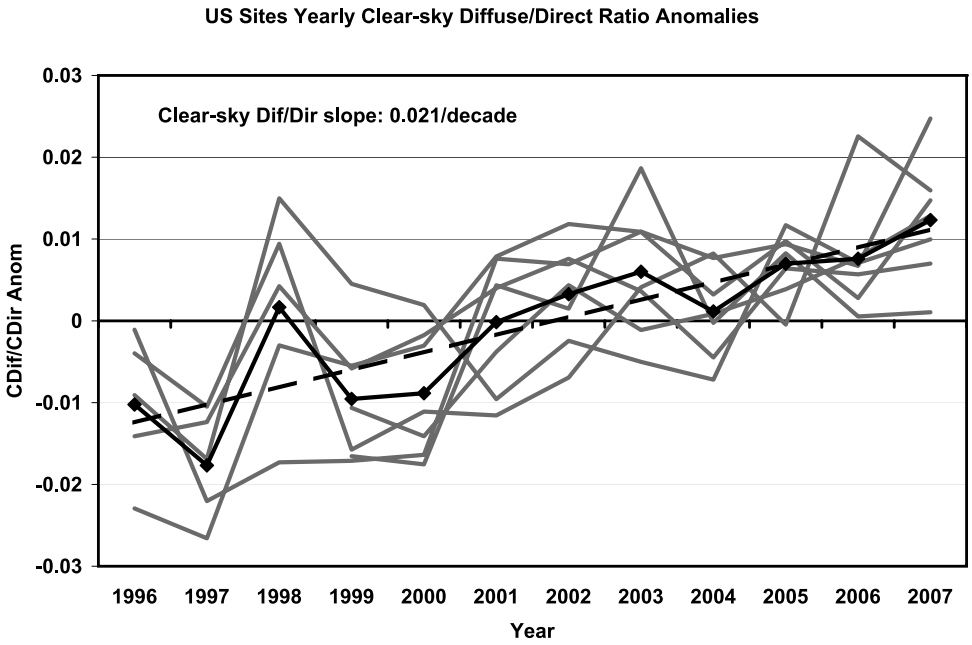

Figure 19. Yearly averages of clear-sky SW diffuse/direct ratio anomalies (gray) for the ARM SGP Central Facility and SURFRAD sites used in this study (see Table 1) as well as the aggregate average (black curve with diamonds) and the corresponding least squares linear fit.

hexagonal columns with optical depth of 0.1 and effective radius of 10 um, the NIP direct component SW is 6% higher than the actual direct beam SW. The increased circumsolar brightness thus entering the field-of-view of the NIP could easily offset any loss due to the small decrease in aerosol optical depth of the *Augustine et al.* [2008] study. Additionally, since the aerosol optical depth retrievals also effectively encompass a field-of-view larger than the solar disk, increased forward scattering could be interpreted as a decrease in optical depth. Yet the same subvisual cirrus would tend to increase the "clear-sky" diffuse SW measurements as well, with the net effect of an increase of the clear-sky total SW as shown in this study. Obviously this explanation is conjecture at this point, and further study is needed. However, one possible source for increased cirrus haze could be increased hydration of the upper troposphere due to increased air traffic. Aircraft jet engines deposit both particulate aerosols and water as part of the jet exhaust.

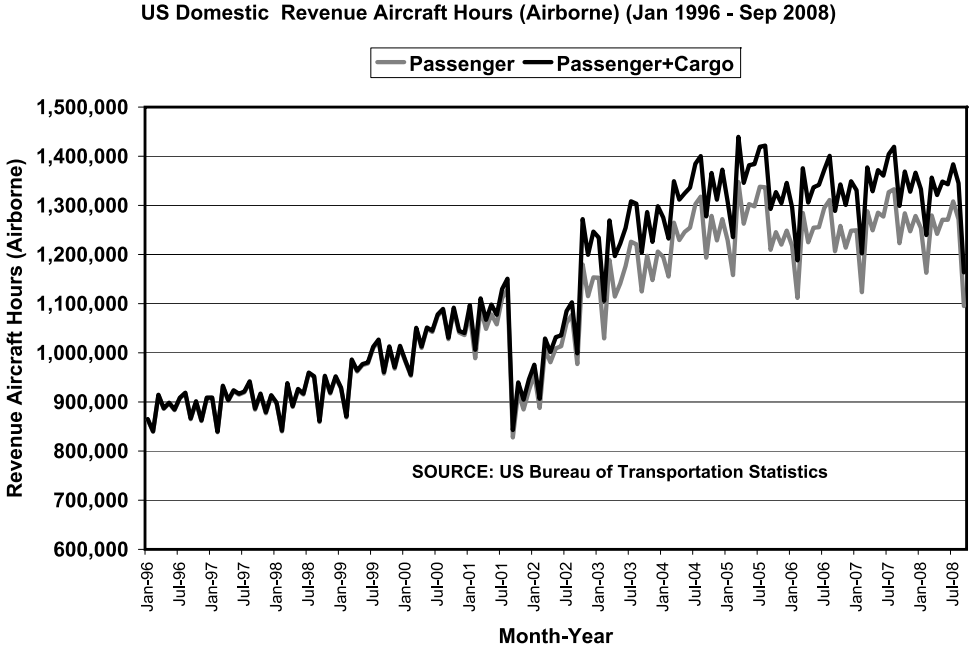

Figure 20. Monthly U.S. domestic aircraft airborne flight hours for the period January 1996 through September 2008 for passenger flights only (gray) and passenger plus cargo flights (black).

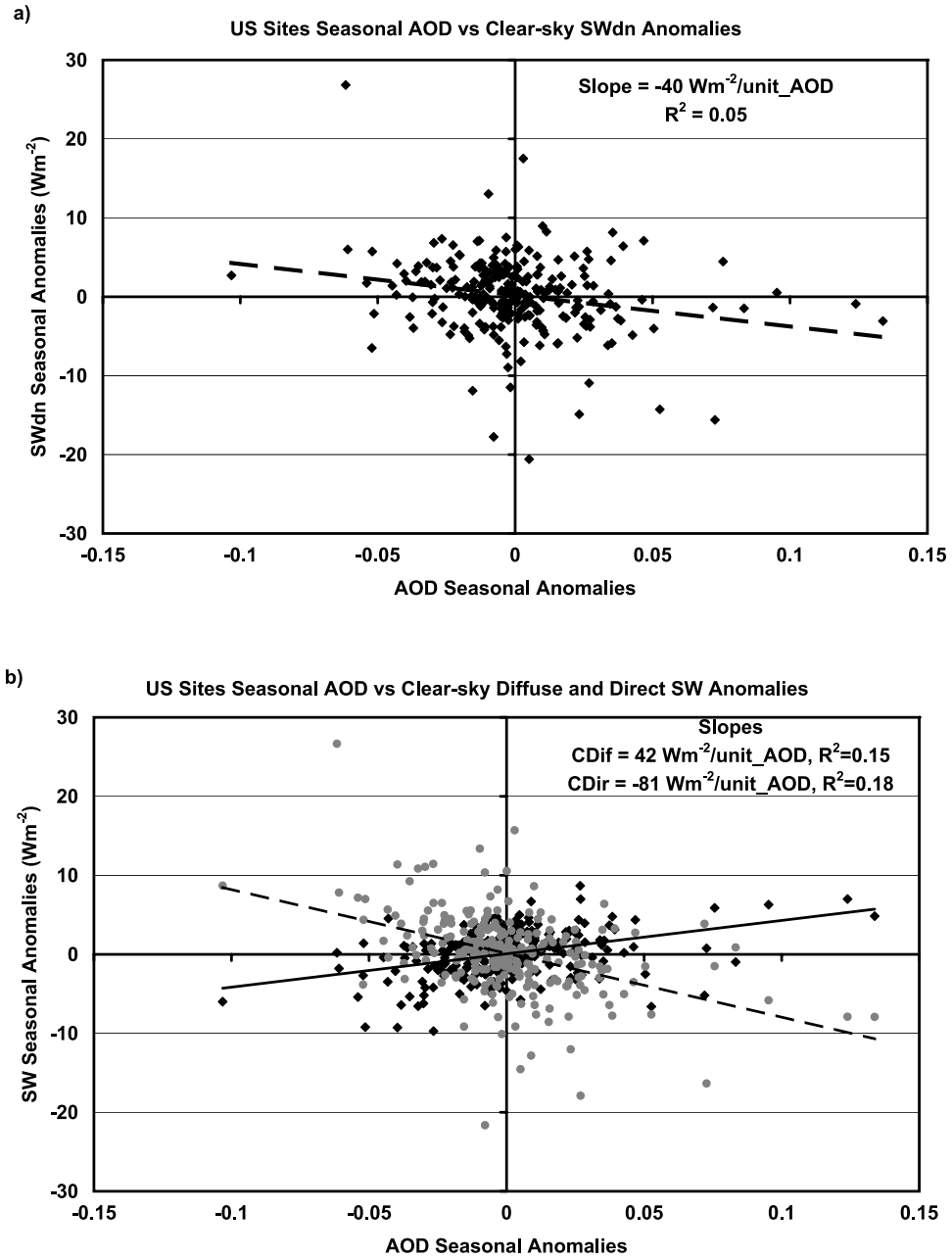

Figure 21. Seasonal anomalies of 500-nm aerosol optical depth versus (a) seasonal anomalies of clear-sky SW and versus (b) the clear-sky diffuse (black) and direct (gray) SW components for the ARM SGP Central Facility and SURFRAD sites used in this study (see Table 1) and the corresponding least squares linear fits.

Figure 20 shows the increase in total flight hours of aircraft over the U.S. from 1996 through 2008, with a drop-off related to 11 September 2001. There have been recent studies indicating increased cirrus due to increased air traffic. *Stubenrauch and Schumann* [2005] show an overall cirrus increase to at least 0.08–0.24% per decade over regions with very high air traffic such as the North Atlantic flight corridor. *Minnis et al.* [2004] use surface observations from 1971 to 1995 to show that cirrus increased significantly over the northern oceans and the United States. *Marquart et al.* [2003] use ECHAM4 (European Centre Hamburg Model) Global Circulation Model calculations to show/predict an increase in global annual mean contrail cover from 0.06% in 1992, to 0.14% in 2015, and to 0.22% in 2050, stating that in the northern extratropics, the enhancement of contrail cover is mainly determined by the growth of aviation. While the contrails and "cirrus" discussed in the above papers are all categorized under the "cloud" classification, whereas our speculation deals with cirrus haze that is typically included in the "cloudless" category, nonetheless these documented increases in cirrus related to increased air traffic lend some credence to the speculation that perhaps there might also be a corresponding increase in cirrus haze.

[25] We have mentioned that the direct effect of aerosols alone cannot explain the changes in the surface SW. To further illustrate this point, we have produced the seasonal anomalies of 500 nm aerosol optical depth (AOD) and sky cover to compare with the relevant seasonal anomalies of downwelling SW. We use seasonal anomalies rather than yearly anomalies because, unlike the practically continuous SW and sky cover data, retrieval of aerosol optical depths is far more prone to data gaps. This is because the measurements require a view of the Sun unblocked by cloud, and in some cases instruments fail for extended periods, both of which preclude producing sufficiently meaningful yearly averages for all sites for all years. Figure 21a compares the seasonal 500 nm AOD anomalies versus the corresponding clear-sky downwelling SW anomalies for the ARM SGP and six SURFRAD sites. While a least squares fitted line shows a tendency for decreasing clear-sky SW with increasing AOD, the R^2 value of 0.05 as well as visual inspection indicates little significance to the relationship. Figure 21b shows that as expected the clear-sky direct SW decreases with increasing AOD, while the clear-sky diffuse increases at about half the magnitude of the direct SW decrease, resulting in the overall decrease in total SW with increasing AOD. Again, the R^2 values of the clear-sky direct and diffuse SW versus AOD least squares linear fits indicate only limited significance to the relationships. Yet for the comparison of sky cover anomalies versus all-sky downwelling SW (Figure 22), the R^2 value of 0.62 and a slope value more than 3 times that of Figure 21, as well as visual inspection suggest a stronger relationship. Additionally, for the 500 nm AOD 81% of the clear-sky SW anomalies fall within 5 W m^{-2} in magnitude, where 80% of the all-sky SW anomalies fall within 10 W m^{-2}; that is, the magnitude of the sky cover relationship to SW is twice that of AOD, despite the clear-sky SW itself being much larger in magnitude than the all-sky SW (Figures 1 and 10). Here again is strong evidence that in our study, it appears that clouds play a larger role in all-sky brightening for the continental United States than do aerosols alone.

6. Summary and Conclusions

[26] We have investigated decadal changes in the surface downwelling SW across the continental U.S. using ARM and SURFRAD data, on the scale typical of global circulation models (100–300 km) using ARM SGP Central and Extended Facilities, and at one point at the ARM SGP Central Facility to investigate seasonal aspects reflected in the yearly averages. We have also attempted to identify aspects of the factors that influence the surface downwelling SW, such as cloud amount, that appear to play a significant role in the changes indicated in the data record in both the clear- and all-sky cases.

[27] The results of the nonparametric Mann-Kendall significance determination give a high degree of confidence that a brightening has occurred for the ARM SGP Central Facility for the period from 1996 through 2007 in both the total and diffuse all-sky SW. The brightening trend during this period in all-sky SW is about 6 W m^{-2}/decade with 5 W m^{-2}/decade coming from the diffuse SW component and, while not statistically significant, a slight increasing tendency for the direct SW. The clear-sky diffuse trend is about 3 W m^{-2}/decade, with approximately no tendency in the clear-sky direct across the study years. The clear-sky SW diffuse/direct ratio, often associated with atmospheric turbidity, exhibits an increase that is significant according to MK testing. During the same period both the SW total and LW effective sky cover exhibit decreasing tendencies, though these do not pass the MK test for linear trend significance. The decreasing sky cover results, supported by the decreasing tendency of the effect of clouds on the downwelling SW, suggest that direct aerosol effects alone cannot explain all changes but that changes in cloud amount are likely playing a role in the changes in all-sky total SW. Even in the clear-sky case, direct aerosol effects alone do not fully explain the results shown for the SW diffuse and direct components, nor the behavior of the SW diffuse/direct ratio. Rather, we speculate that some aspects of the field-of-view of the component measurement instruments and details about the exact definition of "clear sky" might play a role here.

[28] In analyses broken down by season, the results suggest that most of the all-sky total SW brightening occurs in the fall and winter months, with corresponding decreasing tendencies in sky cover the greatest of which occurs in winter. For clear skies, there is a brightening in total SW that is greatest (and statistically significant) in summer and fall. Spring exhibits a marginally statistically significant brightening in clear-sky diffuse SW, and also in clear-sky SW diffuse/direct ratio, with increasing tendencies of clear-sky diffuse SW in all other seasons and in summer and winter for the diffuse/direct ratio.

[29] Looking at four of the ARM Extended Facilities surrounding the SGP Central Facility shows that not all sites exhibit the same tendencies in all variables studied. The variability in all-sky quantities across these essentially global circulation model grid scales (100–200 km) suggests some degree of local influence. Yet there is also a degree of year-to-year overall correlation for these sites suggesting that for cloudiness larger-scale (such as synoptic) factors exhibit a degree of influence as well. In the clear-sky case there is little temporal correlation between the sites suggesting that local influences are significantly contributing to the year-to-year variability. The SGP all-site averages show an increasing (though not statistically significant) tendency for all-sky SW, and a statistically significant increase for clear-sky SW, both at about 4 W m^{-2}/decade with corresponding decreasing tendencies of sky cover.

[30] The results including the SGP Central facility and the SURFRAD sites (an attempt to further investigate the extent of these features around the United States) exhibit significant site-to-site scatter, not surprising given the large distances between sites and differing climate regimes they represent. Nevertheless, in the aggregate all-site averages the majority of the irradiance trend estimates are statistically significant according to MK testing. These all-site average results give an all-sky total SW brightening of about 8 W m^{-2}/decade for the least squares slope (Figure 13). Of this, the all-site average increase of the all-sky diffuse and direct SW components are about equal. Though not statistically significant, an overall decreasing tendency in sky cover is suggested of about 2%/decade for SW total and 1.5%/decade for LW effective sky cover.

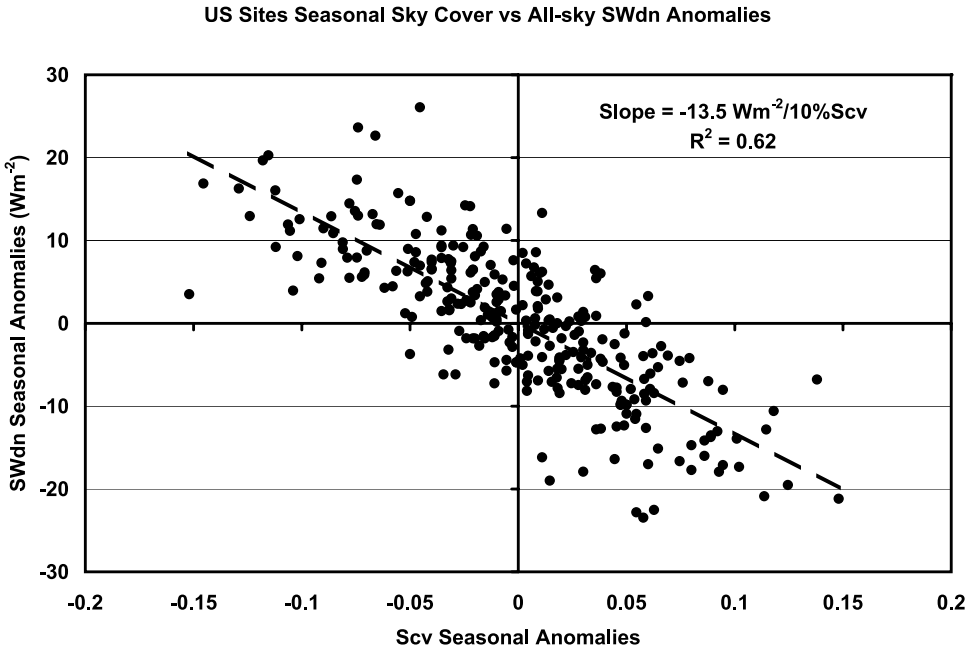

Figure 22. Seasonal anomalies of SW total daylight sky cover (Scv) versus seasonal anomalies of all-sky SW for the ARM SGP Central Facility and SURFRAD sites used in this study (see Table 1) and the corresponding least squares linear fit.

[31] We note that the U.S. 8 W m^{-2} decadal brightening trend estimation is almost three times the magnitude of the *Wild et al.* [2008] reported widespread 2–3 W m^{-2}/decade increase in downwelling longwave over much more of the globe deduced from GEBA records, although this LW slope is about equal to the 95% uncertainty lower bound of our slope determination. The 95% uncertainty range is due, in part, to the limited spatial sampling in both cases. Unlike the *Wild et al.* [2005] 1992–2002 brightening of 6–7 W m^{-2}/decade, our later U.S. trend does not include Mount Pinatubo influences. We also note that documented dimming and brightening are to date not well represented in climate models, as noted by *Wild* [2009] and *Romanou et al.* [2007] in comparing IPCC models with measurements from BSRN sites and ISCCP satellite-derived surface downwelling SW, and as such denotes a significant unresolved problem for climate change prediction.

[32] Clear skies over the ARM and SURFRAD U.S. sites in the aggregate exhibit statistically significant increasing trends of 5 W m^{-2}/decade for both the total and diffuse SW, while the clear-sky direct exhibits no tendency. The clear-sky SW diffuse/direct ratio trend of about 0.02/decade is statistically significant, and is seemingly at odds with recently published results [*Augustine et al.*, 2008] for 1997–2006, although the Augustine *et al.* results are consistent with the clear-sky irradiance trends. We speculate that the AOD and clear-sky diffuse/direct ratio apparently contradictory results might include an increase in subvisual cirrus or other haze phenomena, along with instrument field-of-view characteristics and the limits of condensed water in the atmospheric column allowed under the "clear-sky" categorization of data used in the measurements and retrievals, but obviously further investigation is needed, perhaps more regional and local in nature.

[33] In summary, widespread all-sky and clear-sky SW brightening is shown at sites across the continental United States spanning from 1996 through 2007. The causes of this brightening cannot be solely attributed to changes in dry aerosols or aerosol direct effects, but at least in the all-sky case likely include a cloudiness component contributing to the changes. In the clear-sky case, our results do not support decreasing dry aerosol amounts as the sole cause for increasing total SW, on the basis of statistically significant increasing trends in the clear-sky SW diffuse/direct ratio shown, and the corresponding tendencies in the diffuse and direct SW components. Obviously some other factors are involved.

[34] We also will continue to collect data at these sites to extend the record to investigate future changes and produce the analysis and retrievals from the Radiative Flux Analysis package. This will be used in various ways, for instance by separation of the results by cloud amounts (clear sky, partly cloudy, mostly cloudy, overcast) to further investigate under what circumstances the greatest contributions to the decadal changes of the yearly averages occur. We will also perform seasonal analyses for all sites, as we did for the ARM SGP central facility, to investigate how the year-to-year changes are manifested across the year. Given the apparent local and also larger-scale influences we will approach the determination of the causes of decadal changes in the downwelling solar radiation at the surface on local and regional scales, rather than on global or continental scales. We do note that the Radiative Flux Analysis methodology presents a powerful tool for investigation into the causes of these decadal changes in solar radiation reaching the Earth's surface, especially given the currently available decadal or longer surface radiation data records, though most of these are located in the Northern Hemisphere and all are on land. We agree with the recommendations of the IPCC AR-4 report

that expansion of the number of regionally representative surface sites is sorely needed.

[35] **Acknowledgments.** The authors acknowledge the support of the Office of Science (BER) of the U.S. Department of Energy as part of the ARM Program. The NOAA contributions are supported by the NOAA Climate Goal and the NASA Radiation Projects Office. M. Wild acknowledges the support of the Swiss National Centre for Competence in Climate Research (NCCR Climate). Recognition is also extended to those responsible for the operation and maintenance of the instruments that produced the data used in this study; their diligent and dedicated efforts are often underappreciated.

References

Augustine, J. A., J. J. DeLuisi, and C. N. Long (2000), SURFRAD - A national surface radiation budget network for atmospheric research, *Bull. Am. Meteorol. Soc.*, *81*(10), 2341–2357, doi:10.1175/1520-0477(2000)081<2341:SANSRB>2.3.CO;2.

Augustine, J. A., G. B. Hodges, C. R. Cornwall, J. J. Michalsky, and C. I. Medina (2005), An update on SURFRAD—The GCOS surface radiation budget network for the continental United States, *J. Atmos. Oceanic Technol.*, *22*, 1460–1472, doi:10.1175/JTECH1806.1.

Augustine, J. A., G. B. Hodges, E. G. Dutton, J. J. Michalsky, and C. R. Cornwall (2008), An aerosol optical depth climatology for NOAA's national surface radiation budget network (SURFRAD), *J. Geophys. Res.*, *113*, D11204, doi:10.1029/2007JD009504.

Barnard, J. C., and C. N. Long (2004), A simple empirical equation to calculate cloud optical thickness using shortwave broadband measurements, *J. Appl. Meteorol.*, *43*(7), 1057–1066, doi:10.1175/1520-0450(2004)043<1057:ASEETC>2.0.CO;2.

Barnard, J. C., C. N. Long, E. I. Kassianov, S. A. McFarlane, J. M. Comstock, M. Freer, and G. M. McFarquhar (2008), Development and evaluation of a simple algorithm to find cloud optical depth with emphasis on thin ice clouds, *Open Atmos. Sci. J.*, *2*, 46–55, doi:10.2174/1874282300802010046.

Dupont, J. C., M. Haeffelin, and C. N. Long (2008), Evaluation of cloudless-sky periods detected by shortwave and longwave algorithms using lidar measurements, *Geophys. Res. Lett.*, *35*, L10815, doi:10.1029/2008GL033658.

Durr, B., and R. Philipona (2004), Automatic cloud amount detection by surface longwave downward radiation measurements, *J. Geophys. Res.*, *109*, D05201, doi:10.1029/2003JD004182.

Dutton, E. G., J. J. Michalsky, T. Stoffel, B. W. Forgan, J. Hickey, D. W. Nelson, T. L. Alberta, and I. Reda (2001), Measurement of broadband diffuse solar irradiance using current commercial instrumentation with a correction for thermal offset errors, *J. Atmos. Oceanic Technol.*, *18*, 297–314, doi:10.1175/1520-0426(2001)018<0297:MOBDSI>2.0.CO;2.

Dutton, E. G., D. W. Nelson, R. S. Stone, D. U. Longenecker, G. Carbaugh, J. M. Harris, and J. Wendell (2006), Decadal variations in surface solar irradiance as observed in a globally remote network, *J. Geophys. Res.*, *111*, D19101, doi:10.1029/2005JD006901.

Evans, K. F. (1998), The spherical harmonics discrete ordinate method for three-dimensional radiative atmospheric radiative transfer, *J. Atmos. Sci.*, *55*, 429–446, doi:10.1175/1520-0469(1998)055<0429:TSHDOM>2.0.CO;2.

Gilgen, H., M. Wild, and A. Ohmura (1998), Means and trends of shortwave irradiance at the surface estimated from GEBA, *J. Clim.*, *11*, 2042–2061.

Harrison, L., J. Michalsky, and J. Berndt (1994), Automated multifilter rotating shadow-band radiometer: An instrument for optical depth and radiation measurements, *Appl. Opt.*, *33*, 5118–5125.

Hirsch, R. M., J. R. Slack, and R. A. Smith (1982), Techniques of trend analysis for monthly water quality data, *Water Resour. Res.*, *18*(1), 107–121, doi:10.1029/WR018i001p00107.

Intergovernmental Panel on Climate Change (2007), Summary for policymakers, in *Climate Change 2007: The Physical Science Basis. Contribution of Working Group I to the Fourth Assessment Report of the Intergovernmental Panel on Climate Change*, edited by S. Solomon et al., pp. 4–5, Cambridge Univ. Press, Cambridge, U. K.

Kendall, M. G. (1975), *Rank Correlation Methods*, Charles Griffin, London.

Liepert, B. G. (2002), Observed reductions of surface solar radiation at sites in the United States and worldwide from 1961 to 1990, *Geophys. Res. Lett.*, *29*(10), 1421, doi:10.1029/2002GL014910.

Long, C. N. (2004), The next generation flux analysis: Adding clear-sky LW and LW cloud effects, cloud optical depths, and improved sky cover estimates, paper presented at 14th ARM Science Team Meeting, Dep. of Energy, Albuquerque, N. M.

Long, C. N. (2005), On the estimation of clear-sky upwelling SW and LW, paper presented at 15th ARM Science Team Meeting, Dep. of Energy, Daytona Beach, Fla.

Long, C. N., and T. P. Ackerman (2000), Identification of clear skies from broadband pyranometer measurements and calculation of downwelling shortwave cloud effects, *J. Geophys. Res.*, *105*(D12), 15,609–15,626, doi:10.1029/2000JD900077.

Long, C. N., and K. L. Gaustad (2004), The shortwave (SW) clear-sky detection and fitting algorithm: Algorithm operational details and explanations, *ARM TR-004*, 26 pp., U. S. Dep. of Energy, Washington, D. C. (Available at http://www.arm.gov)

Long, C. N., and Y. Shi (2008), An automated quality assessment and control algorithm for surface radiation measurements, *Open Atmos. Sci. J.*, *2*, 23–37, doi:10.2174/1874282300802010023.

Long, C. N., and D. D. Turner (2008), A method for continuous estimation of clear-sky downwelling longwave radiative flux developed using ARM surface measurements, *J. Geophys. Res.*, *113*, D18206, doi:10.1029/2008JD009936.

Long, C. N., T. P. Ackerman, K. L. Gaustad, and J. N. S. Cole (2006), Estimation of fractional sky cover from broadband shortwave radiometer measurements, *J. Geophys. Res.*, *111*, D11204, doi:10.1029/2005JD006475.

Mann, H. B. (1945), Non-parametric tests against trend, *Econometrica*, *13*, 245–259, doi:10.2307/1907187.

Marquart, S., M. Ponater, F. Mager, and R. Sausen (2003), Future development of contrail cover, optical depth, and radiative forcing: impacts of increasing air traffic and climate change, *J. Clim.*, *16*, doi:10.1175/1520-0442(2003)016<2890:FDOCCO>2.0.CO;2.

McFarlane, S. A., and K. F. Evans (2004), Clouds and shortwave fluxes at Nauru. Part II: Shortwave flux closure, *J. Atmos. Sci.*, *61*, 2602–2615, doi:10.1175/JAS3299.1.

Michalsky, J. J., J. A. Schlemmer, W. E. Berkheiser, J. L. Berndt, L. C. Harrison, N. S. Laulainen, N. R. Larson, and J. C. Barnard (2001), Multiyear measurements of aerosol optical depth in the Atmospheric Radiation Measurement and Quantitative Links program, *J. Geophys. Res.*, *106*(D11), 12,099–12,108, doi:10.1029/2001JD900096.

Michalsky, J. J., G. P. Anderson, J. Barnard, J. Delamere, C. Gueymard, S. Kato, P. Kiedron, A. McComiskey, and P. Ricchiazzi (2006), Shortwave radiation closure studies for clear skies during the Atmospheric Radiation Measurement 2003 Aerosol Intensive Observation Period, *J. Geophys. Res.*, *111*, D14S90, doi:10.1029/2005JD006341.

Minnis, P., J. K. Ayers, R. Palikonda, and D. Phan (2004), Contrails, cirrus trends, and climate, *J. Clim.*, *17*, doi:10.1175/1520-0442(2004)017<1671:CCTAC>2.0.CO;2.

Norris, J. R., and M. Wild (2007), Trends in aerosol radiative effects over Europe inferred from observed cloud cover, solar "dimming" and solar "brightening", *J. Geophys. Res.*, *112*, D08214, doi:10.1029/2006JD007794.

Ohmura, A., and H. Lang (1989), Secular variation of global radiation over Europe, in *Current Problems in Atmospheric Radiation*, edited by J. Lenoble and J. F. Geleyn, pp. 98–301, Deepak, Hampton, Va.

Peppler, R. A., et al. (2008), Quality Assurance of ARM Program Climate Research Facility Data, *DOE/SC-ARM/TR-082*, 65 pp., Dep. of Energy, Washington, D. C. (Available at http://www.arm.gov)

Philipona, R. (2002), Underestimation of solar global and diffuse radiation measured at Earth's surface, *J. Geophys. Res.*, *107*(D22), 4654, doi:10.1029/2002JD002396.

Pinker, R. T., B. Zhang, and E. G. Dutton (2005), Do satellites detect trends in surface solar radiation?, *Science*, *308*, 850–854, doi:10.1126/science.1103159.

Ritsche, M. T. (2006), Surface Meteorological Observation System (SMOS) handbook, *ARM TR-031*, 28 pp., Dep. of Energy, Washington, D. C. (Available at http://www.arm.gov)

Romanou, A., B. Liepert, G. A. Schmidt, W. B. Rossow, R. A. Ruedy, and Y. Zhang (2007), 20th century changes in surface solar irradiance in simulations and observations, *Geophys. Res. Lett.*, *34*, L05713, doi:10.1029/2006GL028356.

Ruckstuhl, C., et al. (2008), Aerosol and cloud effects on solar brightening and the recent rapid warming, *Geophys. Res. Lett.*, *35*, L12708, doi:10.1029/2008GL034228.

Sen, P. K. (1968), Estimates of the regression coefficient based on Kendall's tau, *J. Am. Stat. Assoc.*, *63*, 1379–1389, doi:10.2307/2285891.

Shi, Y., and C. N. Long (2002), Best estimate radiation flux value added product: Algorithm operational details and explanations, *ARM TR-008*, 58 pp., Dep. of Energy, Washington, D. C. (Available at http://www.arm.gov)

Stanhill, G., and S. Cohen (2001), Global dimming: A review of the evidence for a widespread and significant reduction in global radiation, *Agric. For. Meteorol.*, *107*, 255–278, doi:10.1016/S0168-1923(00)00241-0.

Stoffel, T. (2005), Solar Infrared Radiation Station (SIRS) handbook, *ARM TR-025*, 29 pp., Dep. of Energy, Washington, D. C. (Available at http://www.arm.gov)

Streets, D. G., Y. Wu, and M. Chin (2006), Two-decadal aerosol trends as a likely explanation of the global dimming/brightening transition, *Geophys. Res. Lett.*, *33*, L15806, doi:10.1029/2006GL026471.

Stubenrauch, C. J., and U. Schumann (2005), Impact of air traffic on cirrus coverage, *Geophys. Res. Lett.*, *32*, L14813, doi:10.1029/2005GL022707.

Wild, M. (2009), How well do the IPCC-AR4/CMIP3 climate models simulate global dimming/brightening and related effects on twentieth century daytime and nighttime warming?, *J. Geophys. Res.*, doi:10.1029/2008JD011372, in press.

Wild, M., A. Ohmura, H. Gilgen, and D. Rosenfeld (2004), On the consistency of trends in radiation and temperature records and implications for the global hydrological cycle, *Geophys. Res. Lett.*, *31*, L11201, doi:10.1029/2003GL019188.

Wild, M., H. Gilgen, A. Roesch, A. Ohmura, C. N. Long, E. G. Dutton, B. Forgan, A. Kallis, V. Russak, and A. Tsvetkov (2005), From dimming to brightening: Decadal changes in solar radiation at the Earth's surface, *Science*, *308*, 847–850, doi:10.1126/science.1103215.

Wild, M., A. Ohmura, and K. Makowski (2007), Impact of global dimming and brightening on global warming, *Geophys. Res. Lett.*, *34*, L04702, doi:10.1029/2006GL028031.

Wild, M., J. Grieser, and C. Schär (2008), Combined surface solar brightening and increasing greenhouse effect support recent intensification of the global land-based hydrological cycle, *Geophys. Res. Lett.*, *35*, L17706, doi:10.1029/2008GL034842.

Younkin, K., and C. N. Long (2004), Improved correction of IR loss in diffuse shortwave measurements: An ARM value added product, *ARM TR-009*, 50 pp., Dep. of Energy, Washington, D. C. (Available via http://www.arm.gov)

Yue, S., P. Pilon, and G. Cavadias (2002), Power of the Mann-Kendall and Spearman's rho tests for detecting monotonic trends in hydrological series, *J. Hydrol.*, *259*, 254–271, doi:10.1016/S0022-1694(01)00594-7.

J. A. Augustine and E. G. Dutton, Global Monitoring Division, ESRL, NOAA, GMD-1, 325 Broadway, Boulder, CO 80305, USA. (john.a.augustine@noaa.gov; ells.dutton@noaa.gov)

C. J. Flynn, C. N. Long, and S. A. McFarlane, Climate Physics Group, Pacific Northwest National Laboratory, P.O. Box 999, MS K9-24, Richland, WA 99352, USA. (connor.flynn@pnl.gov; chuck.long@pnl.gov; sally.mcfarlane@pnl.gov)

M. Wild, Institute for Atmospheric and Climate Science, Eidgenossische Technische Hochschule, Universitaetsstrasse 16, CH-8092 Zurich, Switzerland. (martin.wild@env.ethz.ch)

W. Wiscombe, Brookhaven National Laboratory, 30 Bell Avenue, Building 490-D, Upton, NY 11973, USA. (wwiscomb@bnl.gov)